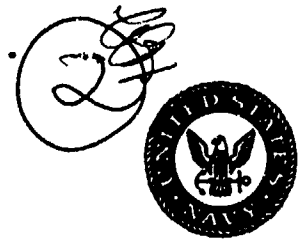

Naval Research Laboratory
Monterey, CA 93943-5006

NRL/FR/7531-92-9413

The Multivariate Optimum Interpolation Analysis of Meteorological Data at the Fleet Numerical Oceanography Center

JAMES S. GOERSS
PATRICIA A. PHOEBUS

Marine Meteorology Division

April 1993

REPORT DOCUMENTATION PAGE

Form Approved
OBM No. 0704-0188

1. AGENCY USE ONLY *(Leave blank)*	2. REPORT DATE	3. REPORT TYPE AND DATES COVERED
	April 1993	Final

4. TITLE AND SUBTITLE

The Multivariate Optimum Interpolation Analysis of Meteorological Data at the Fleet Numerical Oceanography Center

5. FUNDING NUMBERS

Job Order No. 14311A
Program Element No. 0602435N
Project No. RM35G82
Task No. 1
Accession No. DN656756

6. AUTHOR(S)

James T. Goerss and Patricia A. Phoebus

7. PERFORMING ORGANIZATION NAME(S) AND ADDRESS(ES)

Naval Research Laboratory
Marine Meteorology Division
Monterey, CA 93943-5006

8. PERFORMING ORGANIZATION REPORT NUMBER

Formal Report 9413
NOARL Report 31

9. SPONSORING/MONITORING AGENCY NAME(S) AND ADDRESS(ES)

Office of Naval Research, Code 22
800 N. Quincy Street
Arlington, VA 22217-5000

10. SPONSORING/MONITORING AGENCY REPORT NUMBER

11. SUPPLEMENTARY NOTES

12a. DISTRIBUTION/AVAILABILITY STATEMENT

Approved for public release; distribution is unlimited.

12b. DISTRIBUTION CODE

13. ABSTRACT *(Maximum 200 words)*

The operational global database at Fleet Numerical Oceanography Center (FNOC) is the most complete in the world. In addition to conventional radiosonde and surface data, it includes satellite-derived temperature soundings and satellite-derived wind information, along with synthetic observations in the vicinity of extratropical and tropical storms. To take full advantage of this database for improved meteorological analyses and forecasts, significant upgrades were made to the Navy Operational Global Atmospheric Prediction System (NOGAPS) at FNOC in January of 1988. These improvements included the implementation of a global spectral forecast model, a normal-mode initialization, improved data quality control, and a multivariate optimum interpolation (MVOI) analysis scheme. Since that time, the MVOI has become the centerpiece of all the Navy's meteorological data assimilation systems, providing global, regional, and local analysis capability both ashore and afloat.

In a data assimilation system like NOGAPS, the 6-hour model forecast valid at the analysis time is used as the background for the analysis. The analysis, in turn, combines information from the background with the quality-controlled observations to provide updated fields that are used to initialize the forecast model. The MVOI analysis utilizes data from all available platforms to produce analyzed fields that possess minimum error in a statistical sense, while taking into account the error properties of the model forecast used for the background fields and the error properties of the observational data used to update the background. Thus, unlike earlier objective analysis schemes that essentially averaged the nearby data, the MVOI makes some very intelligent decisions about how to treat the various, often conflicting, sources of information it has available.

Three major factors influence the quality of the analysis produced by the MVOI. One is the proper specification of the statistical parameters required by the optimum interpolation methodology. Another is the quality control of the observations themselves. The third is the selection of the appropriate mix of observations to be presented to the analysis. The determination of the statistical parameters required by the analysis is accomplished using a database created for the purpose of monitoring the performance of the MVOI. This same database can be used to monitor the quality of individual observations. In addition, extensive quality control of the data is performed within the MVOI. Finally, the analysis has been designed to take into account the global distribution of observational data, as well as insuring the representative use of the many different data types.

14. SUBJECT TERMS	15. NUMBER OF PAGES
optimum interpolation analysis, data assimilation, NOGAPS	59
	16. PRICE CODE

17. SECURITY CLASSIFICATION OF REPORT	18. SECURITY CLASSIFICATION OF THIS PAGE	19. SECURITY CLASSIFICATION OF ABSTRACT	20. LIMITATION OF ABSTRACT
Unclassified	Unclassified	Unclassified	Same as report

CONTENTS

The Multivariate Optimum Interpolation Analysis of Meteorological Data at the Fleet Numerical Oceanography Center

1.0 Introduction

In simplest terms, the forecast skill of an automated atmospheric prediction system is dependent upon two factors: (1) the ability of the forecast model to realistically depict actual atmospheric processes; and (2) the ability to provide the model with initial conditions that reflect the true state of the atmosphere at scales that are resolvable by the model. The first factor is strictly dependent upon the formulation of the forecast model itself, while the second factor is dependent upon all components of the data assimilation system. To produce the best initial conditions for their forecast models, all operational forecast centers continually run a four-dimensional data assimilation cycle that generally consists of four components: data quality control, data analysis, model initialization, and the forecast model itself.

While the components of the data assimilation system each perform a separate function, they are inextricably connected. Given an estimate of the current state of the atmosphere, the analysis must somehow update this information using current observations. A short-range forecast, initialized from the previous analysis and valid at the current analysis time, provides first-guess, or background, fields for the current analysis. This analysis, in turn, provides the initial fields for the next forecast; hence, the nomenclature data assimilation *cycle*. The forecast model serves as the integrator of past observations, and the analysis serves as the assimilator of current observations. Effective quality control of the observational data is vital prior to the analysis, and even during the analysis itself, to prevent erroneous observations from contaminating the results. Following the analysis, the initialization step adjusts the analyzed fields prior to their use as initial conditions by the forecast model, thereby removing gravity-wave noise that can contaminate the first few forecast hours. If the analysis is performing as an effective component of the data assimilation system, the analyzed fields will closely reflect the information contained in the good observations and the initialization will make only small adjustments to these fields.

Over the past 35 years, the automated analysis of meteorological data has evolved from the relatively simple objective analysis techniques introduced by Bergthórssen and Döös (1955) and elaborated upon by Cressman (1959) to the more sophisticated statistical techniques of the optimum interpolation (OI) methodology first described by Gandin (1963). Although the operational implementation of OI techniques lagged this early theoretical development by over a decade, OI is now used for meteorological data analysis by many of the world's operational forecasting centers (Rutherford, 1976; McPherson et al., 1979; Lorenc, 1981; Mills and Seaman, 1990). Comparisons of some of these analysis systems are given by Daley et al. (1985) and Carr (1987). The evolution

of the U.S. Navy's operational analysis system has followed a similar course. The original successive corrections analysis (Barker, 1982) was replaced by a global multivariate optimum interpolation (MVOI) analysis in 1988 (Barker, 1992; Goerss and Phoebus, 1992). The MVOI was developed by the Marine Meteorology Division of the Naval Research Laboratory (NRL), and is run operationally by the Navy's Fleet Numerical Oceanography Center (FNOC) in Monterey, California.

The MVOI is an integral part of the Navy Operational Global Atmospheric Prediction System (NOGAPS), which basically consists of the four components described above. Along with the changes to the analysis, major upgrades were made to the other system components in 1988, as well. The global grid point model (Rosmond, 1981) was replaced with a spectral forecast model, and the variational initialization was replaced by a normal mode initialization. These components are described in detail by Hogan et al. (1991). Continuous research and experimentation since that time have resulted in further improvements to the various NOGAPS components. The preliminary quality control of the observations is described by Baker (1991), while advances in the initialization and the forecast model are discussed by Rosmond (1992).

This report describes the Navy's operational atmospheric analysis system and documents the status of that system as it existed in April 1991. The global analysis is produced for 16 pressure levels (the 15 standard levels from 1000 mb to 10 mb plus 925 mb) on the Gaussian grid of the NOGAPS spectral forecast model. The Gaussian grid points are separated by 1.5° in the east-west direction and by approximately 1.5° in the north-south direction. The analyzed meteorological variables are geopotential height and the u- and v-wind components. A complete description of the techniques and algorithms used in the MVOI analysis is given in Section 2.0, with an emphasis on the global application of that analysis. Section 3.0 provides a summary of the global meteorological database and discusses how the data are prepared for the NOGAPS analysis. The analysis process itself is described in detail in Section 4.0. Since the MVOI was developed so that with some modification it can be used to satisfy other Navy requirements, we describe these other analysis applications and their associated modifications to the MVOI in Section 5.0. Finally, we will summarize improvements made, to date, and discuss our plans for future upgrades to the data assimilation system.

2.0 Multivariate Optimum Interpolation Analysis

2.1 Theory

In a data assimilation cycle, the data analysis step provides a way of updating a first-guess, or background, field using data that has become available since the last analysis was made. The background field is usually a model forecast, initialized from the previous analysis, that is valid at the synoptic time nearest the new observations. Since the data analysis is actually an estimate of the change in the background field, it typically involves the computation of weighted sums of data

increments, valid at fixed grid points over the area of interest. The data increments are formed by interpolating the background field to the locations of observations and taking the differences between the observed values and the interpolated background values. The analyzed increments are then added to the background values at each analysis point to produce the new estimate of the field. In mathematical notation,

$$F_k^a = F_k^p + \sum_{i=1}^{N} w_{ik} f_i^o , \tag{1}$$

where F represents a full-field variable and f represents an incremental variable. The superscripts a, p, and o distinguish analyzed, predicted (background), and observed values, respectively. The subscript k indicates an analysis grid point location, while the subscript i represents an observation location. Finally w_{ik} is the weight associated with the observed increment f_i^o for the analysis at grid point k. What is unique to the OI methodology is the way the weights w_{ik} are computed.

The OI technique utilizes observed data to compute increments to the background field in such a way that the *mean squared error of the analysis will be minimized* if computed over a statistically significant number of cases. There are some limitations to this optimization, however, due to the various assumptions that must be made, and due to the inexact determination of the statistical parameters that must be specified. These limitations will become more apparent as the discussion continues. The theoretical development of OI is well documented elsewhere (Bergman, 1979; Lorenc, 1981), but for completeness, descriptions of the basic equations will be presented in this section.

Let F_k^t represent the true value of some variable at a given location. While we would like to know F_k^t exactly, at best we can only estimate it from the available sources of information. The predicted value F_k^p provides one such estimate. Through the model forecast, we have information carried along from past observations, modified and controlled by the physical and dynamical constraints of the model itself. From the nearby observations, the F_i^o, we have estimates of the current state of the atmosphere. The objective analysis scheme combines these various sources of information to produce another estimate of F_k^t, which we have designated F_k^a. None of these estimates is likely to exactly represent F_k^t, since each estimate has its own inherent sources of error.

Thus, we can denote the actual error associated with each individual value as

Analysis Error: $E^a = F_k^a - F_k^t$ (2)

Observation Error: $E^o = F_i^o - F_i^t$ (3)

Prediction Error: $E^p = F_k^p - F_k^t$. (4)

In this discussion, we assume that the expected value (or mean) of these errors is zero. Given a large ensemble of similar realizations, we can determine the following statistical error estimates

Analysis Error Estimate $\hat{E}^a = \left\langle (E^a)^2 \right\rangle^{1/2}$ (5)

Observation Error Estimate $\hat{E}^o = \left\langle (E^o)^2 \right\rangle^{1/2}$ (6)

Prediction Error Estimate $\hat{E}^p = \left\langle (E^p)^2 \right\rangle^{1/2}$, (7)

where the angle brackets indicate the ensemble average. We can then normalize the various errors by these error estimates. Thus, in dimensionless form we have

$$\varepsilon^p = E^p / \hat{E}^p \tag{8}$$

$$\varepsilon^o = E^o / \hat{E}^o \tag{9}$$

$$\varepsilon^a = E^a / \hat{E}^a . \tag{10}$$

Similarly, the observation error estimate and analysis error estimate are normalized by the prediction error estimate giving

$$e^o = \hat{E}^o / \hat{E}^p \tag{11}$$

$$e^a = \hat{E}^a / \hat{E}^p . \tag{12}$$

Since we work only with increments from the background field, the observed increment and the analyzed increment will be represented in dimensionless form by

$$f_i^o = \frac{\left(F_i^o - F_i^p\right)}{\hat{E}^p} \tag{13}$$

$$f_k^a = \frac{\left(F_k^a - F_k^p\right)}{\hat{E}^p} . \tag{14}$$

Then, the analysis at a specific point k, for a set of N observations, may be written in the general form shown in equation (1). The analyzed increment f_k^a at point k is given by the summation

$$f_k^a = \sum_{i=1}^{N} w_{ik} f_i^o . \tag{15}$$

By substituting equations (13) and (14) into equation (1), squaring, and taking the ensemble average, we can derive the expression for the error resulting from the analysis at location k in terms of the relationships between the normalized prediction and observation errors. After some manipulation, we can express the normalized analysis error variance at location k as

$$\left(e_k^a\right)^2 = 1 - 2\sum_{i=1}^{N} w_{ik}h_{ik} + \sum_{i=1}^{N}\sum_{j=1}^{N} w_{ik}w_{jk}M_{ij} \tag{16}$$

where

$$h_{ik} = \left\langle \varepsilon_k^p \varepsilon_i^p \right\rangle - \left\langle \varepsilon_k^p \varepsilon_i^o \right\rangle e_i^o \tag{17}$$

$$M_{ij} = \left\langle \varepsilon_i^p \varepsilon_j^p \right\rangle + e_i^o \left\langle \varepsilon_i^o \varepsilon_j^o \right\rangle e_j^o - e_i^o \left\langle \varepsilon_i^o \varepsilon_j^p \right\rangle - \left\langle \varepsilon_i^p \varepsilon_j^o \right\rangle e_j^o . \tag{18}$$

The terms inside the angled brackets are error correlations. For example, $\left\langle \varepsilon_i^p \varepsilon_j^p \right\rangle$ and $\left\langle \varepsilon_i^o \varepsilon_j^o \right\rangle$ represent the prediction error correlation and observation error correlation, respectively, between the observation locations i and j. In practice, the observation error and prediction error are assumed to be uncorrelated, so terms that contain cross-correlations such as $\left\langle \varepsilon_i^p \varepsilon_j^o \right\rangle$ in equations (17) and (18) are equal to zero. We also assume that the errors associated with observations made at different locations are uncorrelated. This assumption allows us to set observation error correlations such as $\left\langle \varepsilon_i^p \varepsilon_j^o \right\rangle$ equal to one for $i=j$, and equal to zero, otherwise. These assumptions simplify the expressions for h_{ik} and M_{ij} to

$$h_{ik} = \left\langle \varepsilon_k^p \varepsilon_i^p \right\rangle \tag{19}$$

$$M_{ij} = \left\langle \varepsilon_i^p \varepsilon_j^p \right\rangle + e_i^o \left\langle \varepsilon_i^o \varepsilon_j^o \right\rangle e_j^o . \tag{20}$$

The computation of M_{ij} for all i, j pairs results in an $N \times N$ matrix $\mathbf{M}$, where the diagonal term on row i is equal to $1 + (\varepsilon_i^o)^2$ and the off-diagonal terms on row i are equal to $\left\langle \varepsilon_i^p \varepsilon_j^p \right\rangle$, that is, the prediction error correlations between location i and the other $N - 1$ observation locations. Similarly, the computation of h_{ik} for all observations results in an N-dimensional row vector $\mathbf{h}_k$ denoting the prediction error correlation between the N observation locations i and the analysis grid point location k.

The key to the OI methodology is to determine the weights w_{ik} that minimize the analysis error variance in equation (16). As with any minimization problem, we take the partial derivatives of equation (16) with respect to w_{ik} for $i = 1, \ldots, N$; equate the derivatives to zero; and

solve the resulting set of N linear equations for the weights. The solution to this problem is

$$\mathbf{w}_k = \mathbf{M}^{-1}\mathbf{h}_k \tag{21}$$

where $\mathbf{w}_k$ is the N-dimensional row vector of weights w_{ik} and $\mathbf{M}^{-1}$ is the inverse of matrix $\mathbf{M}$. In other words, the weight received by observation i for the analysis at grid point k is a function of the normalized observation error, the normalized prediction error correlations between the observation location i and the other $N-1$ observation locations, and the normalized prediction error correlations between the N observation locations and the grid location k. From this development it can be seen that the weights computed for the observations are dependent upon the specification of the observation error estimate $\tilde{E}^o$, the prediction error estimate $\tilde{E}^p$, and the prediction error correlations $\langle \varepsilon^p \varepsilon^p \rangle$.

Before we describe these quantities in more detail, it would be useful to elaborate on the multivariate and three-dimensional nature of the analysis. Essentially, *multivariate* means that all variable types influence the analysis of any one of the variables. In the Navy's MVOI, the analysis variables are geopotential height and the u- and v-wind components (ϕ, u, and v). We use observations of height, wind, and thickness ($\Delta\phi$ – height differences between adjacent analysis pressure levels) to analyze these three variables. The analyzed geopotential height increment at a given location, then, is affected not only by nearby observed height increments, but also by the observed wind and thickness increments. Thus, in equation (1), the lower case f_i^o's do not necessarily represent the same variable type as the upper case F_k^a and F_k^p and, in fact, are usually a mixture of variable types. The analysis is also three-dimensional, which means that the observed increments do not have to be located at the same level as the computed analysis increment. For example, wind increments at 250 mb may influence the height analysis at 200 mb. The coupling of the variables in three-dimensional space is achieved through the specification of the appropriate correlation functions.

2.2 Specification of Statistical Parameters

In this section we describe in detail how the statistical parameters required by the NOGAPS MVOI analysis are specified. Because of the multivariate three-dimensional nature of the analysis, we must specify the prediction error correlations relating different variable types at different horizontal and vertical locations. Thus, we *model* the prediction error correlation, assuming that it can be expressed as the product of vertical and horizontal components. For the horizontal component, the multivariate specification of the prediction error correlations in the analysis is achieved using the relationship described by Buell (1972). The horizontal prediction error correlation model that is specified correlates geopotential height or thickness data at one location with geopotential height or thickness data at another location, and is primarily a function of the horizontal

separation between the two locations. The multivariate coupling is achieved by differentiating the height-height correlation function to derive the appropriate prediction error correlation functions for various *combinations* of ϕ or $\Delta\phi$, u, and v observations. This ensures that the geostrophic relationship between the analysis *increments* of geopotential height and wind is preserved in the extratropics. It does not, however, ensure that the full analyzed fields of geopotential height and wind are in geostrophic balance. The geostrophic and nondivergent constraints are controlled using the parameter method (Daley, 1985) discussed below.

As we have formulated the analysis, the parameters that must be determined are the observation error estimates ($\tilde{E}^o$), the prediction error estimates ($\tilde{E}^p$), and the prediction error correlations $\langle \varepsilon^p \varepsilon^p \rangle$. In general, prediction error represents the amount of error introduced at a particular location due to the inexactness of the forecast model, while observation error includes both instrument error and subgrid-scale sampling errors, where the measurement is simply not representative of features that can be resolved by the model. Given an incremental analysis scheme that is both multivariate and three-dimensional, the prediction error correlations must likewise be defined three-dimensionally for data increments of all different variable types.

Toward this goal, NRL has developed a database that consists of the data increments of height and wind at all levels for all available radiosonde observations. At any given time, 30-day histories of these increments for both the 0000 UTC and 1200 UTC analysis times reside in on-line disk storage. As an example of the information contained in this database, the standard deviations of the 500-mb height increments computed from a 30-day history of 1200 UTC radiosonde observations are plotted in Figure 1 for a selected area. The number of observations available at each radiosonde station is plotted to the right of the standard deviation with the station identifier plotted below. If we overlook small-scale local variability, we see that, in general, the standard deviations increase with increasing latitude, while at the same latitude, the values on the west coast tend to be larger than those on the east coast. However, since the standard deviations are computed from the data *increments*, they reflect both the observation errors and the prediction errors at each observation location. A discussion of how to partition this information into the separate error components is given in two papers (Hollingsworth and Lönnberg, 1986; Lönnberg and Hollingsworth, 1986), which we will henceforth simply refer to as HLH.

Before we can describe how the increments contained in this database are used to estimate the statistical parameters required by the analysis, some further theoretical development is required. From equations (3) and (4) it can be easily seen that the increment for observation i is also the difference between the observation error and the prediction error at the observation location (i.e., $F_i^o - F_i^p = E_i^o - E_i^p$). Thus, taking the product of the increments for observations i and j and averaging over a large ensemble of similar realizations, we have the covariance

$$C_{ij} = \left\langle \left(E_i^o - E_i^p\right)\left(E_j^o - E_j^p\right) \right\rangle = \left\langle E_i^o E_j^o - E_i^p E_j^o - E_i^o E_j^p + E_i^p E_j^p \right\rangle . \qquad (22)$$

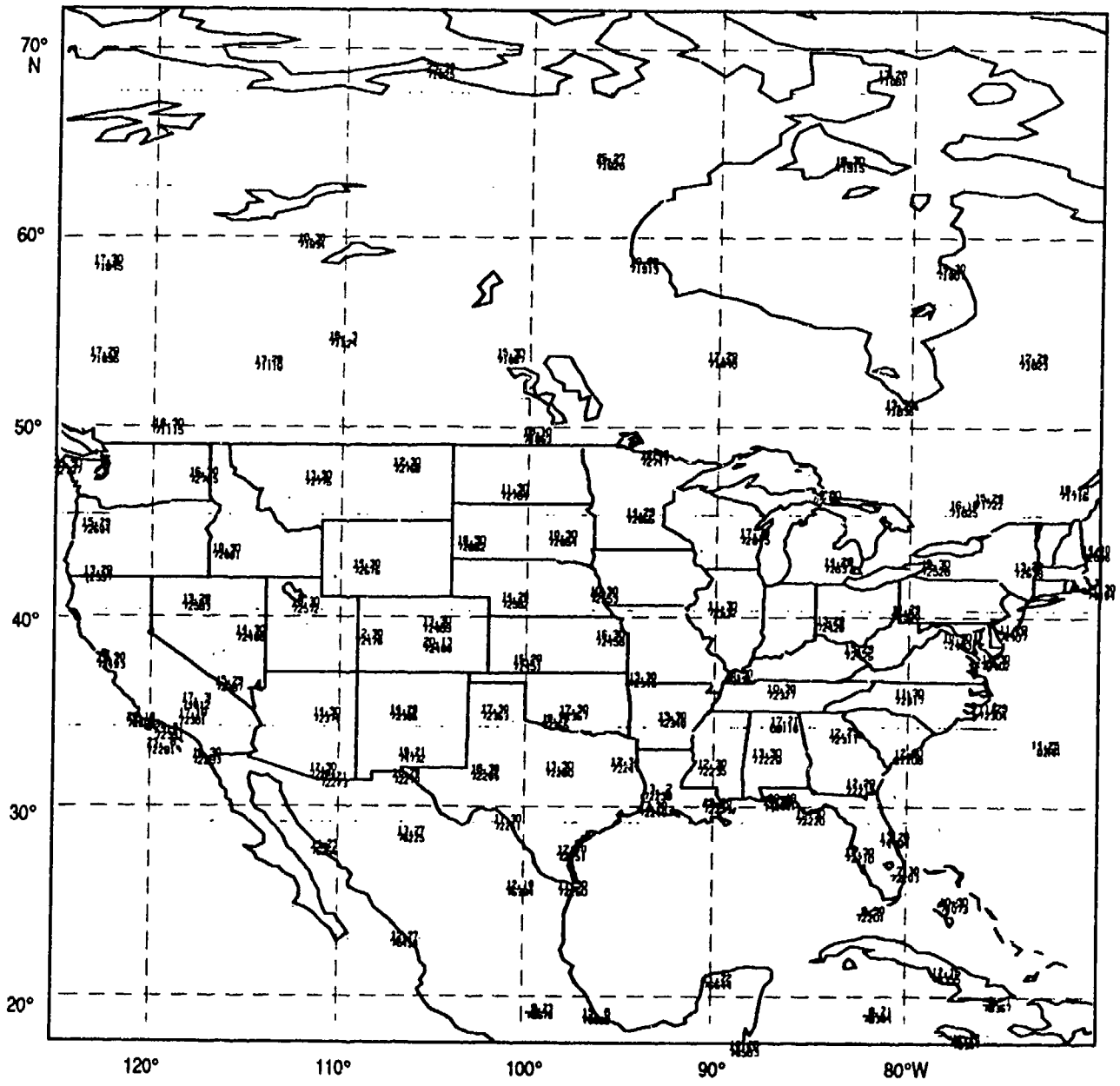

Figure 1. Statistics computed from a 30-day history of 1200 UTC radiosonde observation increments. The 500-mb height increment standard deviation is plotted to the upper left of each station, with the number of available observations plotted to its right. The station identifier is plotted below.

Since we assume that the observation error and prediction error are uncorrelated, the cross-covariance terms vanish. Furthermore, if we limit this discussion to the *horizontal* component of the correlation (i.e., observations i and j are at the same vertical level), we can also assume that the observation errors are uncorrelated. Thus, for i not equal to j, we have

$$C_{ij} = \left\langle E_i^P E_j^P \right\rangle . \tag{23}$$

However, observation error correlation cannot be neglected when $i = j$. Thus, the variance of the increments at location i is given by

$$C_{ii} = \left\langle \left(E_i^o\right)^2 \right\rangle + \left\langle \left(E_i^p\right)^2 \right\rangle = \left(\hat{E}_i^o\right)^2 + \left(\hat{E}_i^p\right)^2. \tag{24}$$

Since we assume that both the observation error and the prediction error have zero mean, we see from equation (24) that the variance of the increments is equal to the sum of the squares of the observation and prediction error estimates. If we further assume that these error estimates do not vary with observation location, we can simply denote the variance of the increments for all observations by

$$C = \left(\hat{E}^o\right)^2 + \left(\hat{E}^p\right)^2. \tag{25}$$

From our database, we can readily estimate the correlation C_{ij}/C. However, this estimate is biased because C contains contributions from both prediction error and observation error. What we want to estimate is the normalized prediction error correlation $\left\langle \varepsilon_i^p \varepsilon_j^p \right\rangle$. But we know that

$$\left\langle \varepsilon_i^p \varepsilon_j^p \right\rangle = \frac{\left\langle E_i^p E_j^p \right\rangle}{\left(\hat{E}^p\right)^2}, \tag{26}$$

and

$$\frac{C_{ij}}{C} = \frac{\left\langle E_i^p E_j^p \right\rangle}{\left(\hat{E}^o\right)^2 + \left(\hat{E}^p\right)^2}. \tag{27}$$

From equations (26) and (27) we see that

$$\frac{C_{ij}}{C} = \left\langle \varepsilon_i^p \varepsilon_j^p \right\rangle \frac{\left(\hat{E}^p\right)^2}{\left(\hat{E}^o\right)^2 + \left(\hat{E}^p\right)^2}. \tag{28}$$

The presence of the square of the observation error estimate in equation (24) biases the correlation estimates obtained from the data by the factor of R, where

$$R = \frac{\left(\hat{E}^p\right)^2}{\left(\left(\hat{E}^o\right)^2 + \left(\hat{E}^p\right)^2\right)}. \tag{29}$$

As observation separation approaches zero, then, the correlation estimate C_{ij}/C will approach R, rather than 1.0 as would be expected. The denominator of equation (29) is simply the variance of the increments.

Thus, if we can determine the value of R, we can compute $(\tilde{E}^p)^2$ and subsequently $(\tilde{E}^o)^2$, thereby partitioning the variance of the increments into the contributions of prediction error and observation error. From the database, we can estimate the horizontal correlations C_{ij}/C for observation increments at various separations. By fitting curves to these results, we can estimate the value of R at each analysis level. The function that best fits the scatter plot of C_{ij}/C versus distance becomes our horizontal height-height correlation function.

The North American continental radiosonde stations are frequently used for these computations because the stations are dispersed over a range of latitudes, the quality of the observations is good, and the instruments used in the U.S. and Canada have similar error characteristics. Thus, from our database, we used the 1200 UTC height increments from March 1990 for an area extending from 25°N to 65°N and from 60°W to 130°W to compute sample estimates of C_{ij}/C at several different analysis levels. Increments for a particular radiosonde station were used in the calculations only if the station reported at least 18 times during the month. Furthermore, only increments that were not rejected by the global MVOI analysis were included. For each station, the mean value of its increments was determined and subtracted from each increment to remove the effects of both observational bias and mean background errors. For each analysis level, horizontal correlation estimates were computed and placed in bins based on the distance between the station pairs. The points plotted in Figures 2 and 3 represent the average

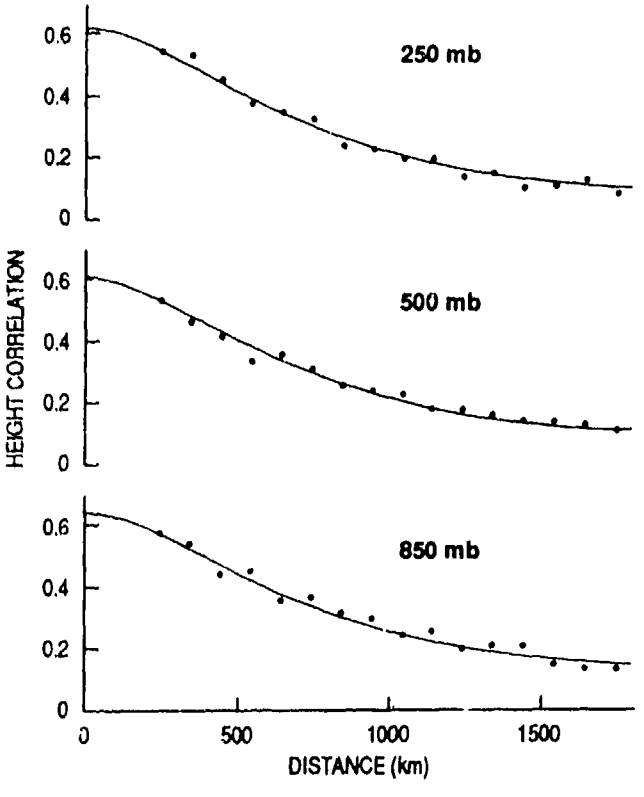

Figure 2. Estimates of the horizontal correlation as a function of distance for radiosonde height increments at 250 mb, 500 mb, and 850 mb.

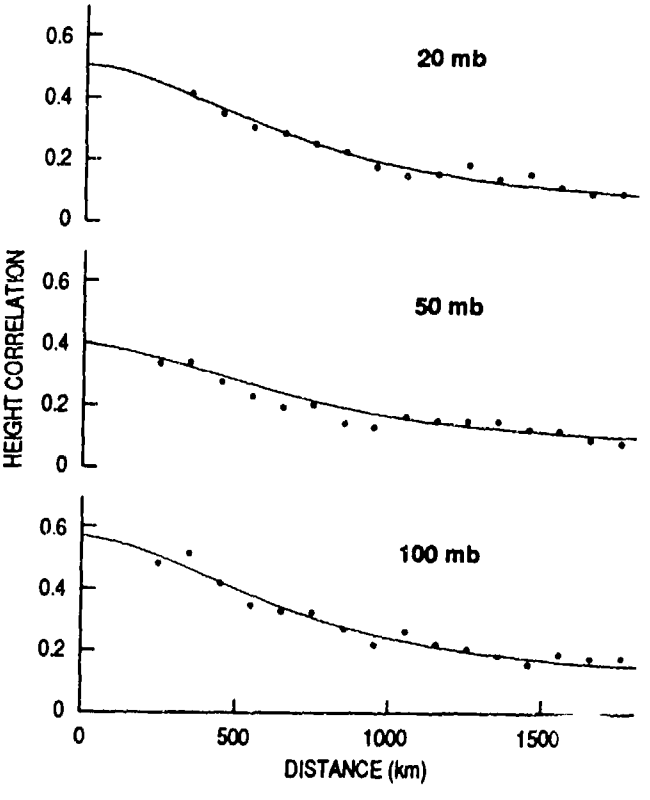

Figure 3. Estimates of the horizontal correlation as a function of distance for radiosonde height increments at 20 mb, 50 mb, and 100 mb.

correlations for 100-km centered bins. Only points where a sufficient number of station pairs were available are shown.

In computing the correlation estimates, we also determined sample estimates of the variance of the increments, C, at each level. To determine the value of R at each level, we must select a correlation function to fit the computed correlations. There are several suitable functions that can be considered. For example, early applications of MVOI in global data assimilation used the negative squared exponential (NSE) function (Bergman, 1979; Lorenc, 1981). As described in HLH, the horizontal correlation function used by the ECMWF is the summation of Bessel functions. More recently, Thiébaux et al. (1990) determined that the optimal correlation function for the NMC global data assimilation system was a third-order autoregressive (TOAR) function. Franke et al. (1988) examined the statistical properties of various functions, including the NSE, second-order autoregressive (SOAR), and TOAR, along with their performance when they were used as the horizontal correlation function for an OI analysis. It was found that the SOAR possessed all of the statistical properties required for an MVOI analysis correlation function and that it could be adequately fitted to correlations estimated from observations. Furthermore, it was found that the quality of the analyses produced using the SOAR were comparable to those produced using the more complicated TOAR and superior to those produced using the NSE. Based on the results of this study and the fact that the SOAR function can be determined with great computational efficiency, we selected the SOAR as the correlation function for the Navy's MVOI analysis.

The suitability of the SOAR function for our system is substantiated by the fit to the radiosonde height data shown by the curves plotted in Figures 2 and 3. The zero-intercept of each curve gives us the value of R at that level. From this value, we can determine the appropriate partition of prediction error and observation error. For example, at 500 mb the sample variance C was 206 m^2. From Figure 2 we can see that $R_{500} = 0.6$. Thus, using equation (29) we can determine that $\tilde{E}^{p}_{500}$ is approximately 11 m and from equation (28) $\tilde{E}^{o}_{500}$ is approximately 9 m. In this way, we obtained the partition of prediction and observation errors for height that are used in the analysis (Fig. 4). We assume that these height prediction errors are applicable at 45°N, the center of the area for which the increment correlations were computed. We also assume that these observation errors are valid only for the radiosonde height data. Observation errors for other data types must be addressed separately, as must the prediction errors for wind data.

While there is some variation in the functions fitted from level to level, we have formulated the analysis to use the same horizontal height correlation function at all analysis levels. In particular, we selected the function fitted to the 500-mb level data shown in Figure 2. To justify the choice of the 500-mb function for all levels, we convert all of the functions shown in Figure 2 and 3 to true correlation functions with a zero-intercept of one (Fig. 5). The fitted 250-mb correlation function is identical to the one fitted at 500 mb. The 850-mb function is slightly broader and is identical to the function fitted at 20 mb. The functions for the lower stratospheric levels (100 mb and 50 mb) are broader still. This broadening is consistent with the results shown in HLH for the

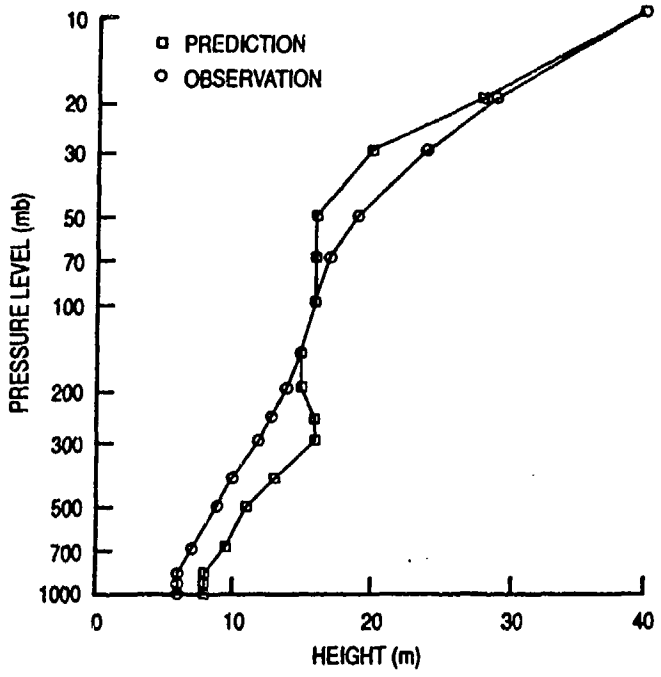

Figure 4. Prediction error and observation error for radiosonde height data at each analysis level.

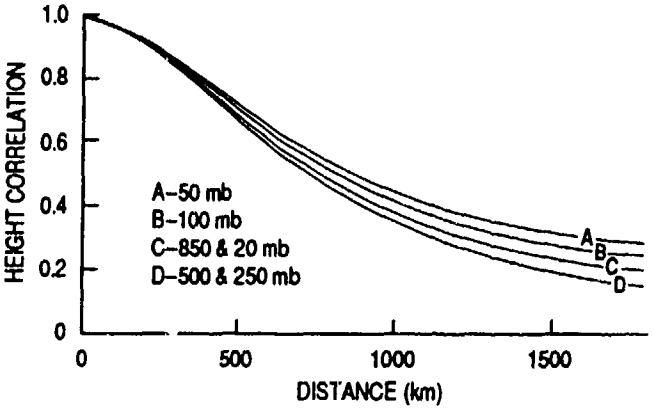

Figure 5. Horizontal correlation functions shown in Figures 2 and 3, after correcting for biases introduced by the observation error.

ECMWF data assimilation system, although they showed a greater contrast between the tropospheric and stratospheric functions.

The exact form of the horizontal correlation function used for height and thickness data in NOGAPS is actually a modified SOAR function given by

$$\langle \phi_i \phi_j \rangle = 1 - c_2 + c_2 (1 + c_1 r_{ij}) \exp[-c_1 r_{ij}], \tag{30}$$

where c_1 and c_2 are constants, r_{ij} is the horizontal (great-circle) distance separating observations i and j, ϕ is the normalized geopotential height, and exp is the exponential function. This normalized correlation function

has a value of 1.0 for co-located observations ($r_{ij} = 0$), and decreases with increasing separation r_{ij}. How rapidly the function decreases is controlled by the values assigned to the constants c_1 and c_2. For the SCRR function fitted to the 500-mb level data in Figure 2, the values for c_1 and c_2 are 2.6 and 0.9, respectively, with the observation separation, r, expressed in units of 1000 km.

The normalized horizontal correlation functions for other data-type pairs are derived from the first and second derivatives of equation (30). Differentiation with respect to r yields

$$\frac{\partial\langle\phi_i\phi_j\rangle}{\partial r} = -c_v^2(r_{ij})\exp\left[-c_1 r_{ij}\right], \tag{31}$$

$$\frac{\partial^2\langle\phi_i\phi_j\rangle}{\partial r^2} = -c_v^2\left(1 - c_1 r_{ij}\right)\exp\left[-c_1 r_{ij}\right]. \tag{32}$$

where

$$c_v^2 = \lim_{r\to 0}\frac{1}{r}\frac{\partial\langle\phi\phi\rangle}{\partial r} = c_1^2 c_2 . \tag{33}$$

The constant c_v is simply the *reciprocal* of the component length scale L_c discussed in HLH. For the ECMWF system, they found tropospheric length scales on the order of 300–350 km and stratospheric length scales on the order of 400–450 km. Thus, the ECMWF analysis is broken into tropospheric and stratospheric layers using different correlation functions that reflect the aforementioned length scales. However, ECMWF found that they must exercise great care in combining the results of the layer analyses to produce the total analysis. For NOGAPS, we found that L_c varied from approximately 400 km at 500 mb and 250 mb to approximately 440 km at 50 mb. This small contrast between the tropospheric and stratospheric length scales in our system indicates that it is quite reasonable to perform a full-depth analysis. Using the current values of c_1 and c_2, we obtain a value of $c_v = 2.47$, which corresponds to a length scale of 400 km. We apply this value at all analysis levels.

Using the derivatives of the height-height correlation model, and converting from natural to rectangular coordinates, the functions correlating the other possible combinations of normalized variables at locations i and j are given by

$$\langle u_i\phi_j\rangle = -\sin\theta\left(\frac{\mu}{c_v}\sqrt{(1-\nu)}\right)\frac{\partial\langle\phi_i\phi_j\rangle}{\partial r}, \tag{34}$$

$$\langle\phi_i u_j\rangle = -\langle u_i\phi_j\rangle \tag{35}$$

$$\langle v_i\phi_j\rangle = \cos\theta\left(\frac{\mu}{c_v}\sqrt{(1-\nu)}\right)\frac{\partial\langle\phi_i\phi_j\rangle}{\partial r}, \tag{36}$$

$$\langle \phi_i v_j \rangle = -\langle v_i \phi_j \rangle \tag{37}$$

$$\langle u_i v_j \rangle = -\sin\theta\cos\theta\left(\frac{1-2\nu}{c_v^2}\right)\left(\frac{1}{r}\frac{\partial\langle\phi_i\phi_j\rangle}{\partial r} = \frac{\partial^2\langle\phi_i\phi_j\rangle}{\partial r^2}\right) \tag{38}$$

$$\langle v_i u_j \rangle = -\langle u_i v_j \rangle \tag{39}$$

$$\langle u_i u_j \rangle = -\left(\frac{1-\nu}{c_v^2}\cos^2\theta + \frac{\nu}{c_v^2}\sin^2\theta\right)\frac{1}{r}\frac{\partial\langle\phi_i\phi_j\rangle}{\partial r}$$

$$-\left(\frac{\nu}{c_v^2}\cos^2\theta + \frac{1-\nu}{c_v^2}\sin^2\theta\right)\frac{\partial^2\langle\phi_i\phi_j\rangle}{\partial r^2} \tag{40}$$

$$\langle v_i v_j \rangle = -\left(\frac{1-\nu}{c_v^2}\sin^2\theta + \frac{\nu}{c_v^2}\cos^2\theta\right)\frac{1}{r}\frac{\partial\langle\phi_i\phi_j\rangle}{\partial r}$$

$$-\left(\frac{\nu}{c_v^2}\sin^2\theta + \frac{1-\nu}{c_v^2}\cos^2\theta\right)\frac{\partial^2\langle\phi_i\phi_j\rangle}{\partial r^2} \tag{41}$$

where θ is the angle of rotation between the rectangular coordinate system and the natural coordinate system whose x-axis lies along the line connecting observation locations i and j. The parameters μ and ν control the geostrophic coupling and divergence, respectively. Both μ and ν range from 0 to 1, with $\mu = 1$ representing full geostrophic coupling of the wind/height correlations and $\nu = 0$ representing fully rotational flow. Outside the tropics, we currently set $\mu = 0.9$ and $\nu = 0$. In the tropics, the geostrophic constraint is relaxed ($\mu = 0.5$) and the divergence is permitted to be nonzero ($\nu = 0.1$). Plots of sample correlation functions for the various data-type pairs in the extratropics are shown in Figures 6(a–f). For comparison, the same functions are shown in Figures 7(a–f), but with the values of μ and ν modified for the tropics.

Estimating the vertical correlation function is not quite as straightforward as determining the horizontal correlation function. Due to the way that we have formulated the MVOI, a single vertical correlation function is used for both height and wind data. While wind observations have little or no vertical correlation of observation error, radiosonde height observations possess strong vertical observation error correlations. Therefore, the assumptions that lead to the definition of C_{ij} in the horizontal case do not apply here. For observations at levels k and l at the same horizontal location, instead of equation (23), we obtain from equation (22)

$$C_{kl} = \langle E_k^o E_l^o \rangle + \langle E_k^p E_l^p \rangle . \tag{42}$$

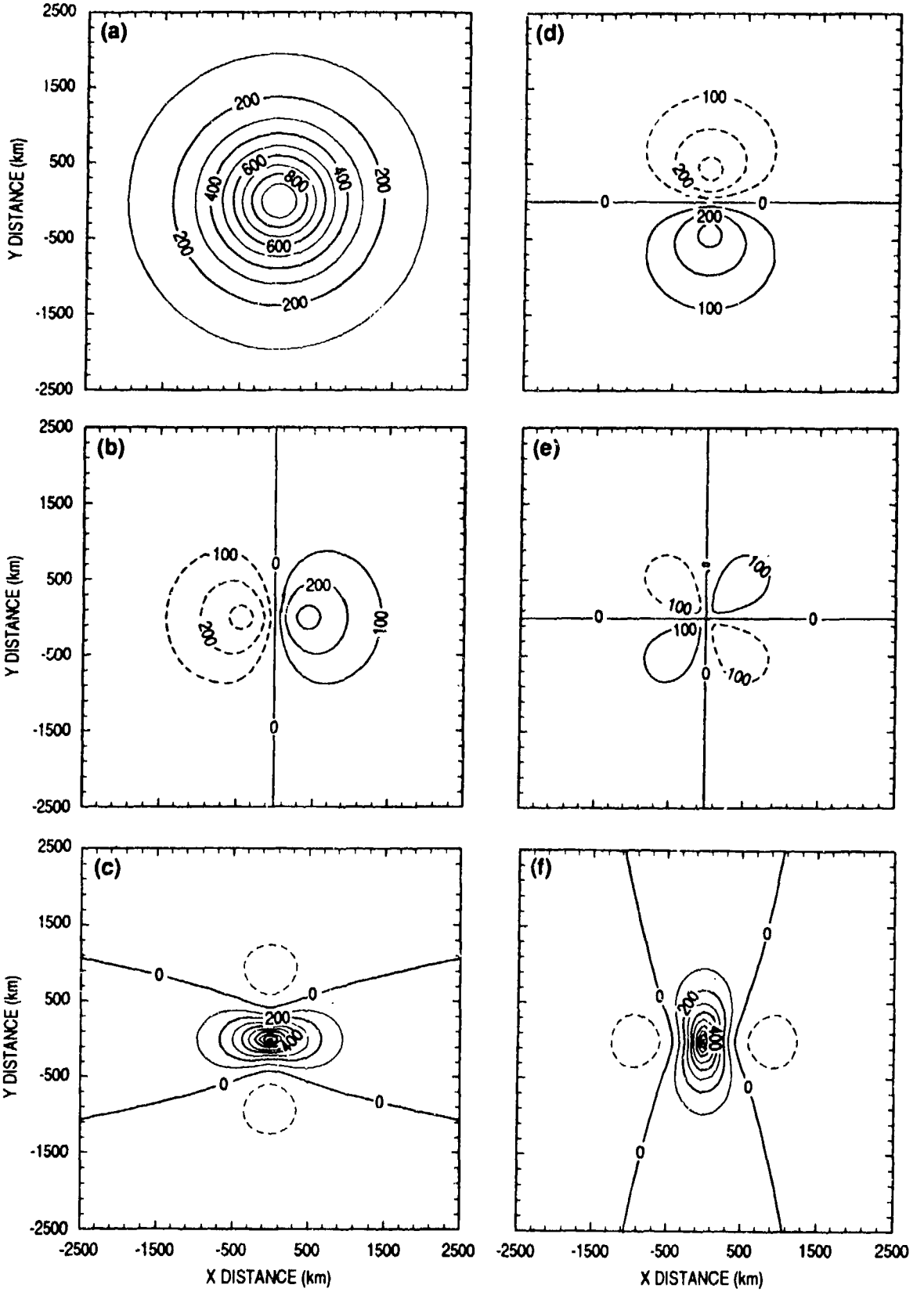

Figure 6. Horizontal components of the prediction error correlation functions used in the NOGAPS MVOI extratropical analysis, assuming $\mu = 0.9$ and $\nu = 0.0$. (a) $\langle \phi\phi \rangle$, (b) $\langle \phi u \rangle$, (c) $\langle \phi v \rangle$, (d) $\langle uv \rangle$, (e) $\langle uu \rangle$, and (f) $\langle vv \rangle$.

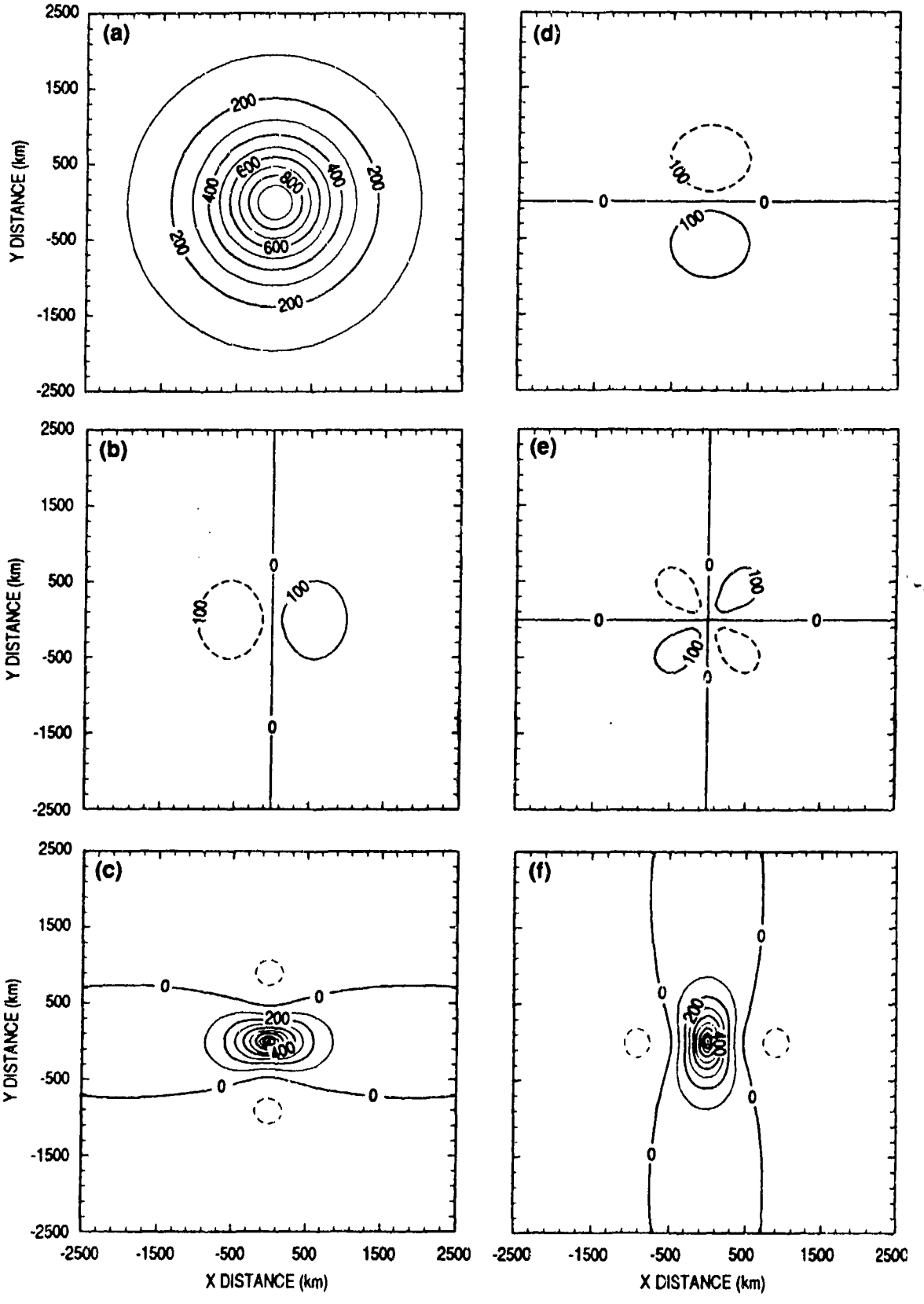

Figure 7. Horizontal components of the prediction error correlation functions used in the NOGAPS MVOI tropical analysis, assuming $\mu = 0.5$ and $\nu = 0.1$. (a) $\langle \phi\phi \rangle$, (b) $\langle \phi u \rangle$, (c) $\langle \phi v \rangle$, (d) $\langle uv \rangle$, (e) $\langle uu \rangle$, and (f) $\langle vv \rangle$.

Multiplying each term in equation (42) by 1,

$$C_{kl} = \frac{\langle E_k^p E_l^p \rangle}{\hat{E}_k^p \hat{E}_l^p} \hat{E}_k^p \hat{E}_l^p + \frac{\langle E_k^o E_l^o \rangle}{\hat{E}_k^o \hat{E}_l^o} \hat{E}_k^o \hat{E}_l^o . \tag{43}$$

Then,

$$C_{kl} = r_{kl}^p \hat{E}_k^p \hat{E}_l^p + r_{kl}^o \hat{E}_k^o \hat{E}_l^o , \tag{44}$$

where r_{kl}^p and r_{kl}^o are estimates of the vertical prediction error correlation and vertical observation error correlation, respectively, between levels k and l. These two correlation estimates are the only quantities in equation (44) that we cannot readily estimate from the aforementioned database. We then assume that the vertical observation error correlation can be represented by

$$r_{kl}^o = (0.95)^n , \tag{45}$$

where n is the absolute value of the difference between integer levels k and l. Substituting equation (45) into equation (44), we solve for the vertical prediction error correlations for height. The radiosonde increment database is used to compute estimates of the vertical correlation functions for height and wind. Figure 8 displays the estimated

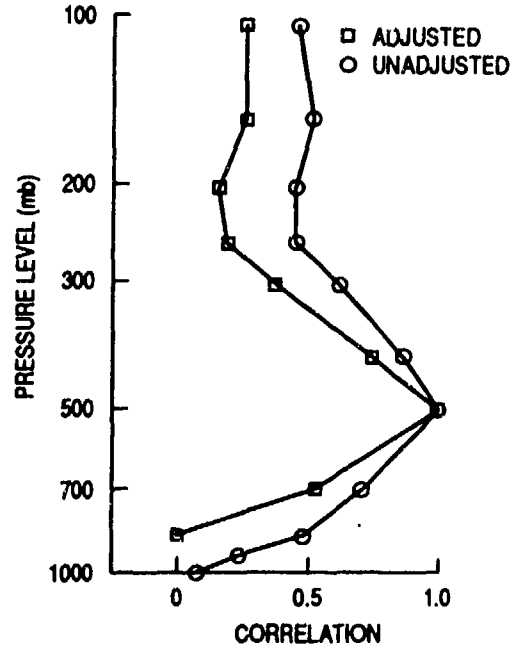

Figure 8. The estimated height correlation function for an observation located at 500 mb, along with the adjusted function obtained by taking into account the vertical correlation of height observation error.

height correlation function for an observation located at 500 mb, along with the adjusted function obtained by taking into account the vertical correlation of height observation error. Figure 9 shows the adjusted height correlation function plotted alongside the estimated vertical wind component correlation function. Since we must select only one vertical correlation function, the function we have chosen represents a compromise between the two correlation function estimates, as depicted in Figure 9.

The curves plotted in Figures 8 and 9 are discrete, rather than continuous, curves. The particular form that we have chosen for the vertical correlation function is a simple exponential function whose shape and magnitude were determined from the actual data. It is represented by

$$S_{ij}^{z} = \exp\left[-\left(\frac{(z_i - z_j)}{d}\right)^{b}\right], \tag{46}$$

where b and d are predetermined constants, equal to 1.8 and 3600, respectively; z_i and z_j are the standard heights in meters at the analysis pressure levels nearest the observations for 300 mb and above, and some specified value that is less than the standard height for locations at 400 mb and below. This modification of the standard heights is made at lower levels to force the vertical correlation to drop off more rapidly, thus better decoupling the boundary layer from the lower and middle tropospheric levels. As stated, the same vertical model is used

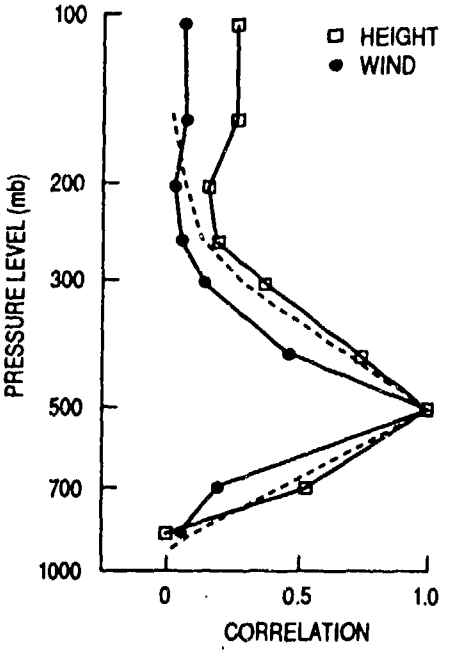

Figure 9. Comparison of the vertical correlation function used in the analysis (dashed line) with the adjusted height correlation function from Figure 8 and the estimated vertical wind component correlation function.

for geopotential height and wind data. However, if one of the variables under consideration is a thickness observation, the vertical model is modified accordingly by using the two bracketing heights (Lorenc, 1981). Figure 10 illustrates the vertical correlation function computed in reference to an observation at 500 mb, using equation (46).

Once the horizontal and vertical components of the correlation function have been determined, the total prediction error correlation for any variable at location i with any ϕ, u, v, or $\Delta\phi$ data at location j is given by

$$S_{ij} = S_{ij}^{r}\, S_{ij}^{z}\,, \tag{47}$$

where S_{ij}^{r} is the horizontal correlation function appropriate for the data-pair type. It should also be noted that in equations (30)–(47), the observation location j could just as easily be the grid location k. In other words, the same expressions are used to compute correlations between observation locations and analyzed grid point locations.

To maintain the geostrophy of the correlation functions for the normalized variables defined in equations (30)–(41), Lorenc (1981) pointed out that the following relationship must be satisfied

$$\hat{E}_{\phi}^{p} = \frac{\mathcal{F}\hat{E}_{u}^{p}}{c_v}\,. \tag{48}$$

This constraint provides us with a formula for computing the prediction errors for the wind components $\left(\hat{E}_{u}^{p}\right)$ from the prediction errors for

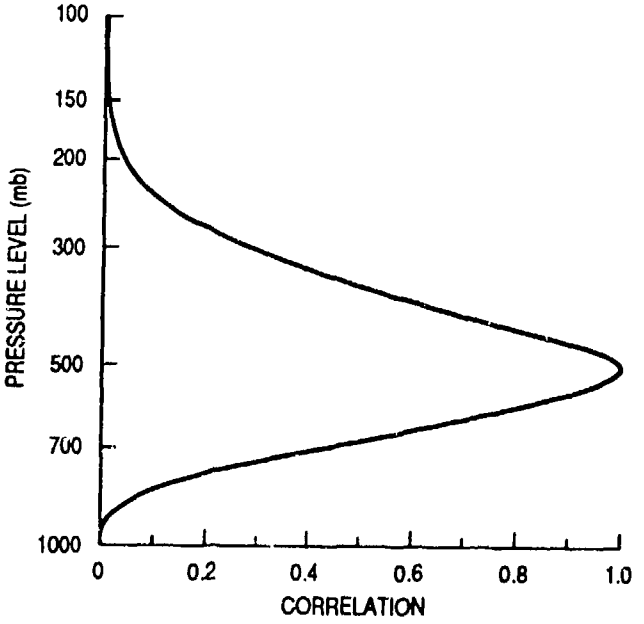

Figure 10. The continuous representation of the vertical correlation function used in the analysis, computed relative to an observation at 500 mb using b = 1.8 and d = 3600.

height $\left(\tilde{E}_{\phi}^{p}\right)$ that were derived from the radiosonde database. The prediction errors for the wind components plotted in Figure 11 were computed from those plotted for height using the Coriolis parameter $\mathcal{F}$, that is valid at 45°N. For comparison, the partitioning of the wind observation and prediction errors was done in the same fashion as was done for the heights, at least in the troposphere and lower stratosphere where the radiosonde increments were available. At most levels, the results obtained by deriving the prediction errors for the wind components from those for height show good agreement with what would have been obtained by performing the partitioning process for wind components. At the higher stratospheric levels, where the analysis background is more greatly influenced by the top level of the NOGAPS forecast model, this agreement breaks down. At these upper analysis levels we have chosen to use wind component prediction errors that are consistent with the height prediction errors and to assign observation errors that are typical of other stratospheric levels.

To complete the specification of the statistical parameters for the MVOI, we must determine values for the observation errors for the different types of observational data used by the analysis. A detailed description of the various data types and their global distribution is presented in the next section. We have already shown how the observation errors for radiosonde data are determined. The magnitude of the observation error for other types of data is also estimated by examining the statistical properties of their differences from the analysis background and taking into account the contribution of the prediction error to these statistical estimates. The resulting observation error estimates for the different data types are summarized in Table 2 in the next section. These estimates

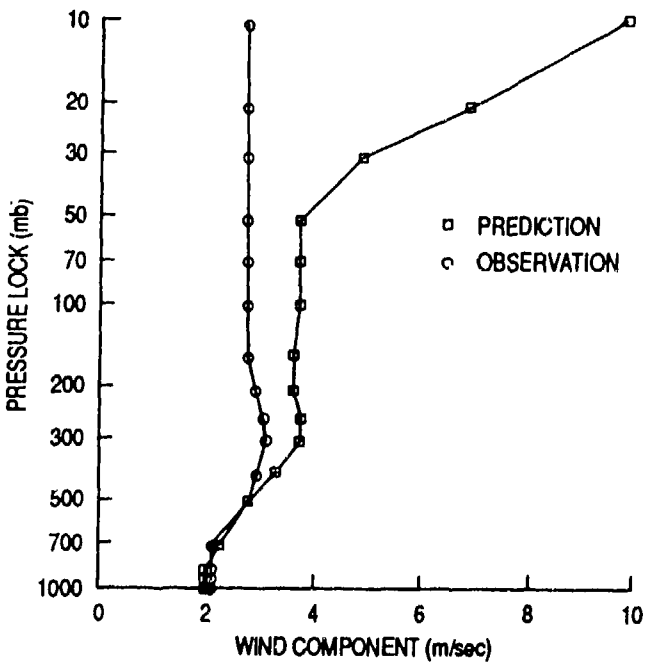

Figure 11. Prediction error and observation error for radiosonde wind data at each analysis level.

are consistent with those described by Shaw et al. (1987) for the ECMWF data assimilation system. In most cases, the observation errors are assumed to be horizontally homogeneous, that is, they do not vary from one x, y location to another.

3.0 Data Processing

The historical evolution of the global database utilized by the world's meteorological forecast centers is described by Dey (1989). With only a few exceptions, all operational forecast centers have access to the same observational data. Atmospheric measurements are made by radiosondes, pilot balloons, aircraft, ships, buoys, and ground stations. Satellite-derived measurements are made using polar-orbiting and geostationary satellites. Synthetic observations are created to provide information in data-sparse areas. In this section we will describe the different types of observations used by the Navy's atmospheric analysis systems, their distribution in space and time, and the types of processing required to prepare the data for the MVOI analysis.

The observations reside in FNOC data files using packed formats that are described in the FNOC Computer User's Guide (1987). Prior to the analysis, data preprocessing software accesses these files and rewrites the observations in the FGGE* format. This standardization of format permits the analysis software to be easily executed using either operational or research data sets.

The data preprocessing that takes place prior to the analysis performs several different quality tests on the data (Baker, 1991), including checks for location, timeliness, and vertical consistency. As a result of these checks, each piece of information is associated with a flag that indicates whether that observation should be rejected, subjected to further checking, or accepted as is. In some cases, the flag value will indicate that a particular correction was made or that the observation was not checked at all. These quality flags are written with the observations in the FGGE format, and are used by the analysis to make additional quality control decisions.

Within the analysis, each data type undergoes further processing. The FGGE-formatted data are read and, if necessary, the reported observations are converted to observations of geopotential height, wind, or geopotential thickness. The observed increments are computed by subtracting the background values from the observed values. Some of the high-resolution observations are thinned and averaged before they are used in the analysis. Certain known errors are corrected, and the preliminary quality flags are used to further assess and assign analysis quality flags to the observed increments. While all data types have some processing steps in common, they also have their own unique set of requirements, so each data type will be discussed in more detail.

3.1 The Global Database

3.1.1 Radiosonde Data

The radiosonde is still the backbone of the observational network, providing twice-daily measurements of atmospheric temperature, moisture, and (indirectly) wind from the surface to the upper stratosphere at fixed

*First GARP Global Experiment (GARP was the Global Atmospheric Research Program).

sites around the globe. From these measurements, observations of geopotential height are computed at the standard pressure levels, and observations of temperature, dew-point depression, wind speed and wind direction are determined at both standard and significant levels. Typically, over 700 radiosonde stations report each day for 0000 UTC and 1200 UTC, while about 50 soundings are received for 0600 UTC and 1800 UTC. The radiosonde network is shown in Figure 12. While the northern midlatitudes are reasonably well covered by these observation sites, there are relatively few stations scattered over the rest of the world. For example, approximately 90% of the radiosonde sites are in the Northern Hemisphere, and only a little over 10% of the stations are located in the tropics. The vertical distribution of radiosonde observations is also non-uniform. While tropospheric coverage is quite good, with 80% of the soundings normally reaching 100 mb, coverage of the stratosphere is less reliable. Only about 40% of the reported soundings reach 20 mb and as few as 10–15% reach 10 mb.

The total number of reports that may be read into the analysis is 1000, which is sufficient to include the 700 or so World Meteorological Organization (WMO) stations, plus ship soundings and synthetic observations. As these reports are read, the reported latitudes and longitudes are checked to remove any duplicates. Only mandatory-level height and wind data are retained, with one exception. Since one of the analysis levels (925 mb) is not a mandatory level, a 925-mb observation is created from two bracketing significant-level observations reported between 1000 mb and 850 mb. If only one such significant level is available, either the 1000 mb or 850 mb report may be used for the other level. If there are no significant-level observations in that range, the 925-mb observation is set to missing, since there is no new information gained by interpolating between two mandatory-level observations. The interpolation is linear with respect to pressure, and heights are processed independently of the wind speed and direction.

A radiation correction is applied to the height reports obtained from the U.S. and the Canadian radiosondes. The appropriate corrections for each country were determined from the radiosonde increment database, described in Section 2.2, and from the results of the international comparison of radiosonde instruments conducted by the WMO at Wallops Island (Nash and Schmidlin, 1987). The magnitude of the corrections is a function of sun angle. The sun angle is determined from the station latitude and longitude; the month, day, and time of day of the sounding; and the balloon ascent rate.

Other types of corrections are also made to certain radiosonde observations. For example, the height reports from China are corrected for observed systematic biases. The magnitude of this bias is determined from the radiosonde increment database, and the correction made always increases the reported height at each pressure level. This correction is imposed on all stations using block numbers beginning with 50–59. Finally, while we do not correct for the Indian height reports at this time, we do flag all height reports from blocks 42 to 43 as suspect.

After the height corrections are made, all height observations are converted to geopotential height and the u- and v-wind components are computed from the wind speed and direction. For all wind data,

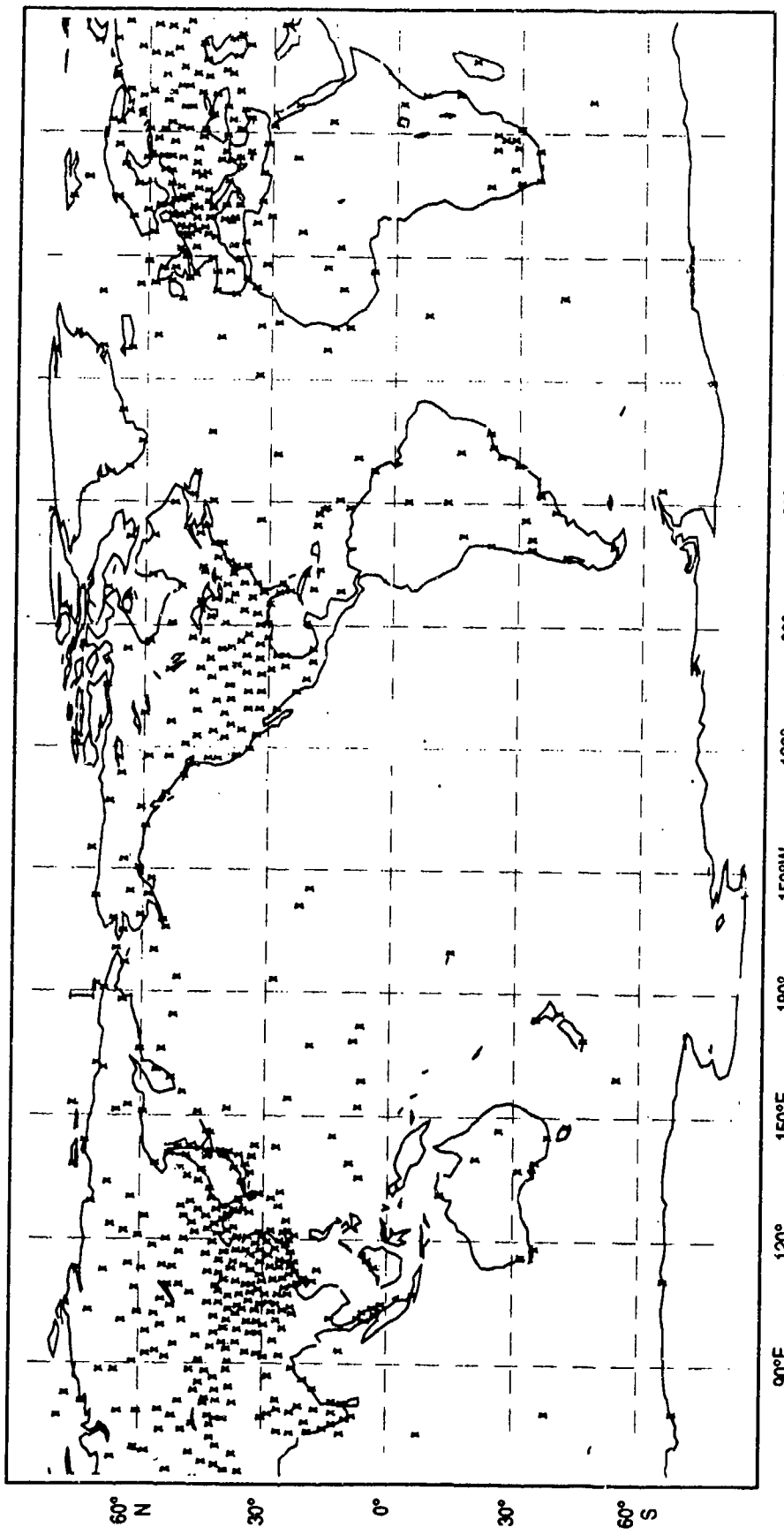

Figure 12. Global distribution of radiosonde observations.

if the reported speed is greater than some predefined limit, the wind components are flagged for rejection. The upper limit is a function of level, and varies from 60 m/sec at 1000 mb to 160 m/sec at 400 mb and higher levels. Using these test results and the quality flags assigned to the variables by the preliminary checks, the analysis quality flag is set to indicate which data have been rejected. Otherwise, the analysis quality flag will reflect the preliminary flag values assigned to the height and wind observations.

The *analysis* quality flag consists of a two-digit number and is illustrated in Table 1. In general, the 10's digit indicates which variables are available, and the 1's digit indicates which variables should be checked further by the analysis. If height and wind data are available at a particular x, y, z location, the 10's digit is set to –1. If only the height report is available, the 10's digit is 0, while wind-only observations are represented by a 10's digit equal to 1. If a particular variable was flagged for rejection by the preceding quality control checks, that variable is considered to be *unavailable* when the value of the analysis quality flag is determined. If the entire observation (all variables at a given location) is to be rejected outright, the analysis quality flag is set to 99. If all the variables in the observation are accepted by the preliminary quality tests, the one's digit of the analysis quality flag is set to 0. Data requiring further checking by the analysis are indicated by setting the 1's digit equal to 1 for the height observation, 2 for the wind components, or 3 for all the variables. *The same convention for the analysis quality flag is followed for all data sources.*

3.1.2 Pilot Balloon Data

Pilot balloons (pibals) also provide vertical soundings of wind speed and direction, but do not generally provide the depth of information available from the radiosondes. Only about one-third of the pibal soundings reach as high as 100 mb. Furthermore, on a global scale, their numbers are relatively small, with 150–200 pressure-level soundings available at each analysis time. However, their spatial distribution is evenly divided

Table 1. MVOI analysis quality flag.

Data Available*	Flag Value	Accept	Check Further	Reject
ϕ only	0	ϕ	—	—
	1	—	ϕ	—
	99	—	—	ϕ
u, v only	10	u,v	—	—
	12	—	u,v	—
	99	—	—	u,v
ϕ,u,v	–10	ϕ,u,v	—	—
	–11	u,v	ϕ	—
	–12	ϕ	u,v	—
	–13	—	ϕ, u,v	—
	99	—	—	ϕ, u,v

*Some values rejected earlier may be considered unavailable.

between the hemispheres, with almost half of the sounding sites located in the tropics (Fig. 13). In this respect, they are an important supplement to the radiosonde network.

Storage space is available in the analysis for up to 650 pibals, which is more than sufficient to handle all the available soundings. Pibals are wind-only soundings that are reported at either fixed pressures or at fixed heights, but not both. Only the mandatory pressure-level observations are saved for the analysis. If the sounding is reported at fixed heights, the 600-m and 900-m wind speeds and directions are vertically interpolated to create a 925-mb wind observation; no other wind observations are used from the height-level soundings. In all cases, wind speeds greater than some predefined limit are ignored. That limit ranges from 60 m/sec at 1000 mb to 160 m/sec at 300 mb and above. The observations exceeding these limits are flagged for rejection. The analysis quality flags for the other observations simply reflect the decisions made by the preliminary quality checks.

3.1.3 Surface Data

Conventional surface observations are those taken by land stations, fixed and drifting buoys, coastal marine stations, and ships. Since surface observations are reported more frequently than upper-air observations, the number of reports is more constant with time, with around 7000 conventional surface observations available at each of the primary analysis times (0000 UTC, 0600 UTC, 1200 UTC, and 1800 UTC). Approximately 90% of these surface reports are from land stations. Although 10 times greater in number than the radiosonde stations, the spatial distribution of the surface stations is similarly skewed toward the Northern Hemisphere (Fig. 14). This is true not only of the land stations, but the marine reports as well. For example, of the 700 or so ship and buoy observations received each analysis time, nearly 90% are located in the Northern Hemisphere. The variables normally reported by the surface platforms include sea-level pressure, temperature, moisture, wind speed and wind direction. A very small percentage of land stations report station pressure or the height of a standard pressure surface rather than sea-level pressure.

As the data are read, duplicate reports are identified by comparing latitudes, longitudes and block/station names. Reports at the same location or with the same identifier are removed (except for observations with generic station names, such as SHIP, BUOY, etc.). Thus, only one observation per platform is used in the analysis, even if that platform reports every hour. Since the data records for the analysis time are read first, followed by observation records at ± 1, ± 2, then ± 3 hours from the analysis time, the most timely observation from each platform is saved. We allow up to 8000 surface reports to be stored, which is sufficient to handle the typical number of reports (around 7000).

The treatment of the wind data is fairly straightforward. First, surface wind observations over land are not used in the analysis. Such observations are too often unrepresentative of the wind in the free atmosphere because of the effects of terrain or shallow radiation inversions. Marine winds flagged for rejection by the preliminary quality checks are assigned an analysis quality flag indicating rejection, and the wind components are set to missing. Wind reports with speeds of greater than

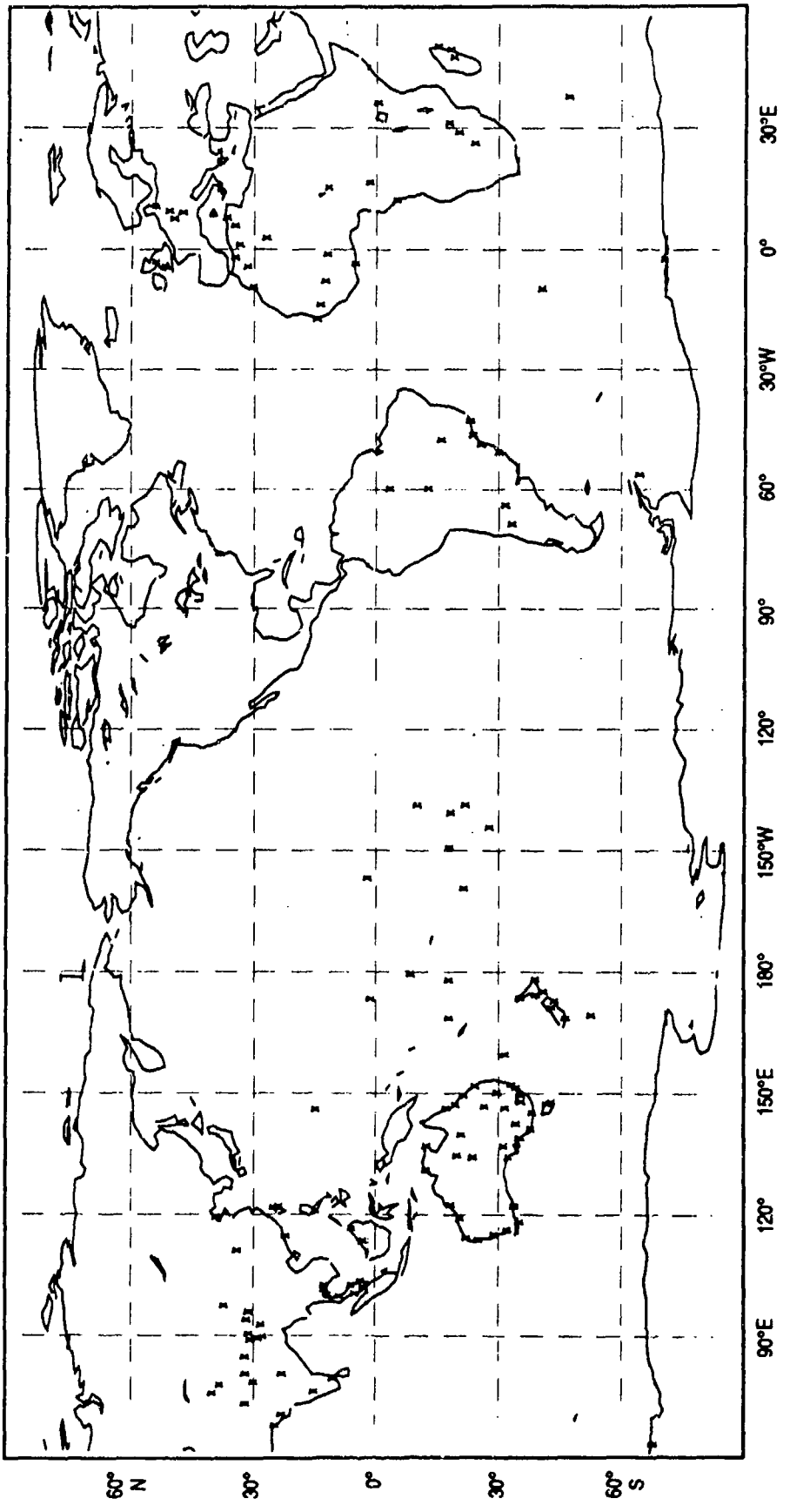

Figure 13. Global distribution of pilot balloon observations.

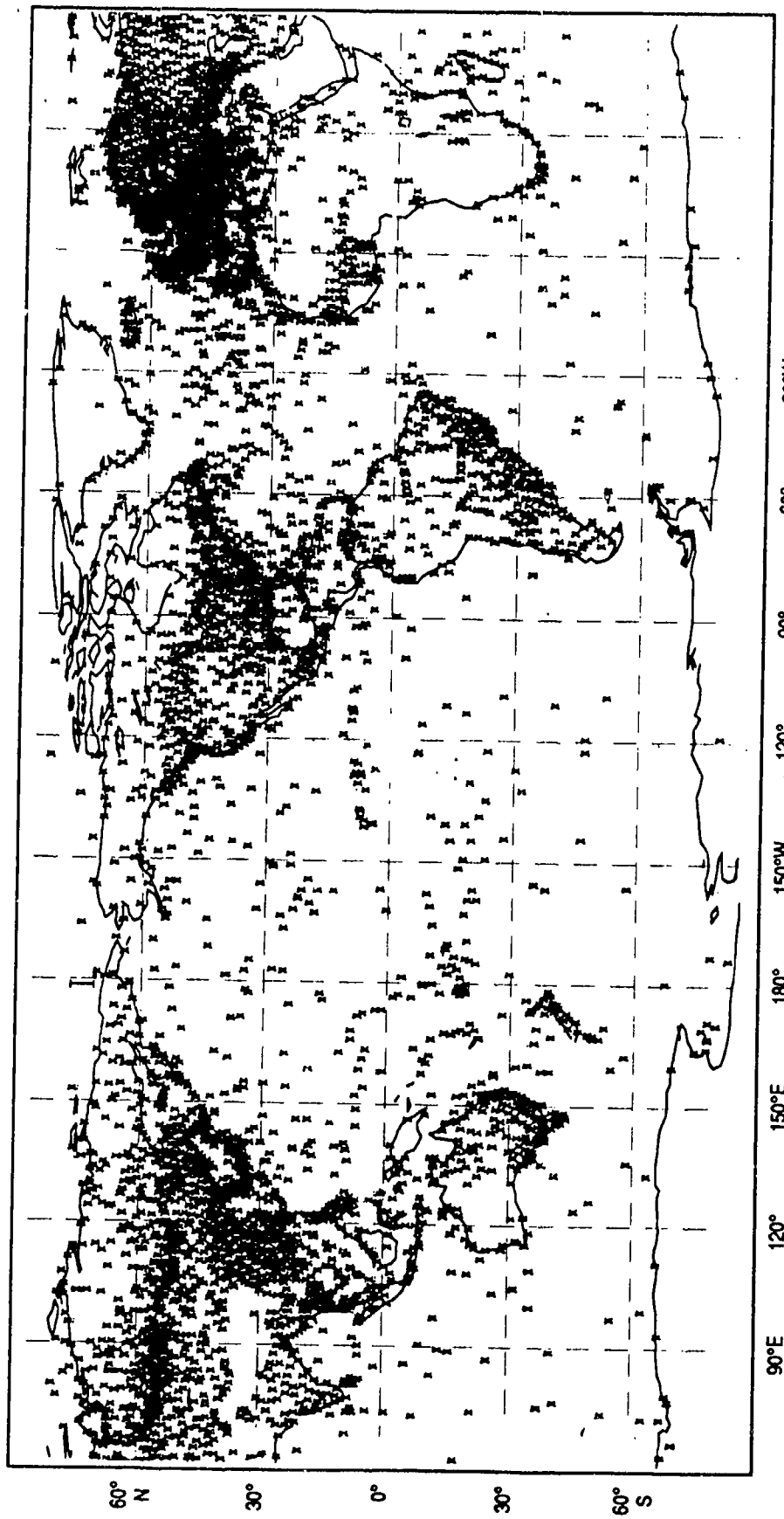

Figure 14. Typical distribution of surface land, ship, and buoy observations for one analysis time.

50 m/sec are similarly rejected. Otherwise, as long as the wind direction is valid (between 0° and 360°), the u- and v-wind components are computed from the reported speed and direction.

Specification of a geopotential height observation from the surface data is more complex, since the various types of surface observations are reported in different ways. Generally, land stations and marine platforms report sea-level pressure. A 1000-mb geopotential height observation is computed from the sea-level pressure using the hypsometric equation, where the layer temperature is assumed to be the reported surface temperature. The reported pressure must be between 920 mb and 1080 mb and the surface temperature between −80°C and 50°C, or the data is flagged for rejection. An added complication arises, since FNOC stores only the last two digits of the surface pressure. Thus, 50 could represent either 950 mb or 1050 mb, with no indication of which is correct. Thus, the alternative pressure is carried along with each observation and is also converted to a 1000-mb height. After the observations are differenced with the background, a decision is made as to which of the alternative values is the correct one.

Over land, some stations report station pressure and elevation. Observations reporting elevations of less than −400 m or greater than 4000 m above sea level are flagged for rejection. Otherwise, the elevation is used to assign the observation to the nearest *analysis* level. To calculate geopotential height at the reported elevation, we first estimate the standard atmosphere pressure at the station's elevation (following Haltiner and Martin, 1957) and compare it to the reported pressure. This comparison resolves discrepancies that may result by assigning the wrong 100's digit to the two-digit pressure report. If the station elevation is less than 437 m, the report is assigned to the 1000-mb analysis level. In this case, if the absolute difference from the standard atmosphere is more than 50 mb, the reported pressure is adjusted by 100 mb in the appropriate direction. At elevations of 437 m and higher, if the pressure difference is more than 100 mb, the reported pressure is incrementally reduced by 100 mb until the difference from the standard pressure at that elevation is less than 100 mb. If the remaining difference is still more than 50 mb, one final 100-mb adjustment is made to the pressure, with the direction of the adjustment determined by the sign of the difference. Finally, the height of the standard atmosphere is determined hydrostatically from the standard pressure at the station's elevation. The difference between the reported elevation and the computed standard height is added to the standard height *for the assigned analysis level*, thereby extrapolating the estimated *increment* at the reported elevation to create an observation of geopotential height at the assigned analysis level. The observation retains the preliminary quality flag of the reported station pressure, and the analysis quality flag is determined accordingly.

Finally, rather than reporting station pressure or estimating the equivalent sea-level pressure, some of the stations at higher elevations report geopotential height at the nearest mandatory pressure level—either 850 mb, 700 mb, or 500 mb. In these cases, since these pressure levels are also analysis levels, no further modification to the reported data is necessary.

3.1.4 Aircraft Data

Aircraft reports include both pilot reports and automated reports. Regardless of their source, all aircraft reports contain single-level wind speed and direction, with the location of each report identified by latitude, longitude, and height above sea level. As can be seen from Figure 15, most of these reports are concentrated along the transoceanic and U.S. transcontinental flight paths. Although most of these observations are taken at cruising altitudes, typically from 300 mb to 200 mb, occasional reports are received at lower or higher levels.

In practice, reports that are less than 500 m above sea level are ignored, as are reports of wind speeds greater than 125 m/sec. Otherwise, the u- and v-wind components are computed from the wind speed and direction, and the preliminary quality flags are used to set the analysis quality flag for each wind report pair. A maximum of 2000 u, v pairs can be stored, with approximately 1000 observation pairs available for each analysis time. Since a number of aircraft follow the same flight paths and tend to report at certain fixed latitude/longitude crossings, the data are thinned by computing time-weighted averages from the co-located aircraft wind observations. This reduces the number available at any one analysis time to around 800.

After the wind components have been computed and stored, but before the wind increments are computed, the observations are sorted—first on latitude, then longitude, followed by height and time. This order ensures that duplicate observations will be stored adjacent to one another in the data arrays and can be easily compared. Duplicate reports, that is, observations reporting identical wind information at the same time and same x, y, z location, are effectively removed from the data set by flagging all but one of them as rejected reports. If two or more observations are reported at the same time and same location, but the reported wind speeds and directions are different, the entire co-located group of observations is flagged for rejection. However, if multiple reports at the same location have the same winds but are reported at different times, the most recent report is assumed to be valid and the others are flagged for rejection. It is not unusual to remove over 150 observations during the duplicate check.

To reduce the redundancy of reports made by different aircraft at different times, but along the same flight path, co-located observations are combined into one *superob* by performing a time-weighted average of the u- and v-wind components individually. The weighting function is of the form

$$\frac{1}{2}\cos\left(\frac{\pi t}{3}\right)+\frac{1}{2}, \tag{49}$$

where t ranges from –3 to +3 hours from the analysis time. The resulting wind components are computed as linear combinations of the original observations and their respective normalized weights. The original observations are then flagged for rejection and replaced with the newly computed superobs of the u- and v-wind components. Normally, 150–200 superob pairs are created, with the majority resulting from the combination of two or three individual reports. However, we have seen superobs computed from up to eight co-located aircraft observations.

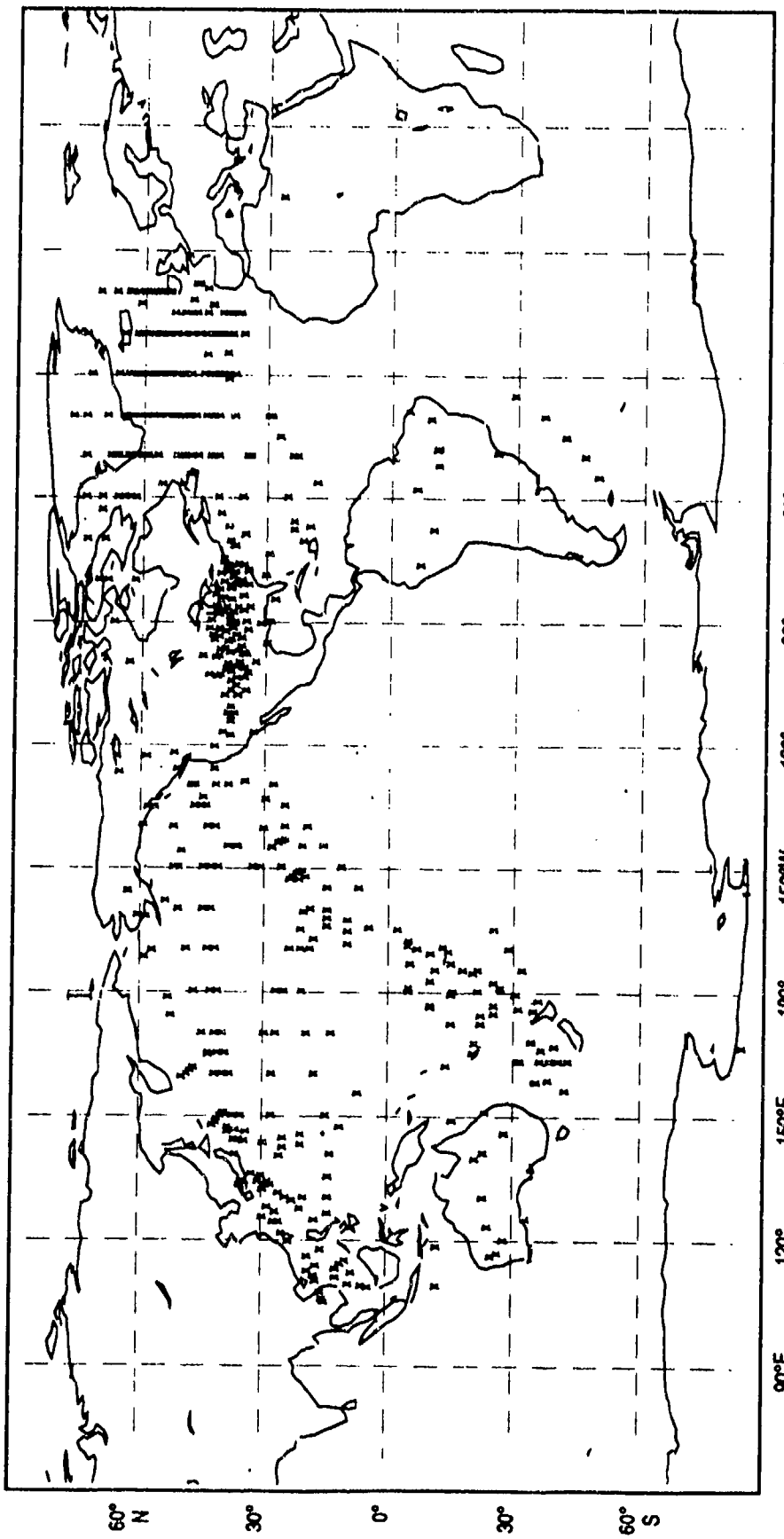

Figure 15. Typical 6-hour availability of aircraft observations for all analysis levels.

3.1.5 Satellite Cloud-Tracked Wind Data

Other single-level wind observations are available from U.S., European, and Japanese geostationary satellites. These data are referred to as cloud-tracked winds, indicative of the method used to derive them. Because of the fixed position of the satellites, it is only possible to accurately produce cloud-tracked winds in the tropics and midlatitudes, between about 50°N and 50°S. While the number of cloud-tracked winds is more variable than other types of single-level observations, 1000–2000 are usually available for the 0000 UTC, 0600 UTC, and 1200 UTC analysis times. The distribution of these observations is obviously dependent upon cloud coverage, but they are fairly evenly distributed between the hemispheres, with roughly half of the observations located in the tropics (Fig. 16). The cloud-tracked winds tend to be vertically clustered, with around 50% reported below 775 mb and about one-third of the reports concentrated at jet levels (300–200 mb). The remainder of the reports are scattered at various levels, up to approximately 100 mb.

Up to 6000 cloud-tracked wind observations, valid within 3 hours of the analysis time, can be stored for the analysis, with typical numbers around 1500. Observations with a reported pressure greater than 1000 mb or less than 10 mb are excluded. Reported wind speeds of greater than 125 m/sec are disregarded. Observations flagged as erroneous by the preliminary quality-control checks are assigned an analysis quality control flag of 99, for rejection. Remaining observations are checked for appropriate ranges of values for wind speed, direction, and location, with any out-of-range value causing an observation to be flagged for rejection.

3.1.6 Satellite Sounding Data

Satellites also provide multilevel observations in the form of temperature soundings that are derived from radiance measurements made by the polar orbiters. FNOC has access to data from four such satellites, two flown by the National Oceanic and Atmospheric Administration (NOAA-10 and -11) and two from the Defense Meteorological Satellite Program (DMSP F8 and F9). However, if desired, data from any individual satellite can be excluded, without software changes, simply by specifying the proper input parameters in the job stream that executes the analysis. Data from the remaining satellites will not be affected. With all four satellites available, global coverage is provided every 6 hours. Figure 17 shows the typical coverage available for an analysis time. With few exceptions, each satellite sounding extends from the surface to at least 10 mb, with the NOAA satellite soundings extending to 0.4 mb. In addition, the NOAA satellites provide measurements of precipitable water from the surface to 300 mb.

Up to 4360 soundings can be stored for use in the analysis. Since this is less than the number of available soundings over a 6-hour analysis window, every fourth sounding is skipped as the data are read, thereby reducing the number of profiles while retaining good horizontal coverage. Each sounding, as it is passed to the analysis, contains multiple reports of layer thickness in geopotential meters. Each thickness report is accompanied by a quality flag and by the pressures at the top and bottom of the layer. If the layer so defined coincides with a layer defined by the analysis pressure levels, the report is saved for the analysis. The only test performed on the data (at this stage) assures that the

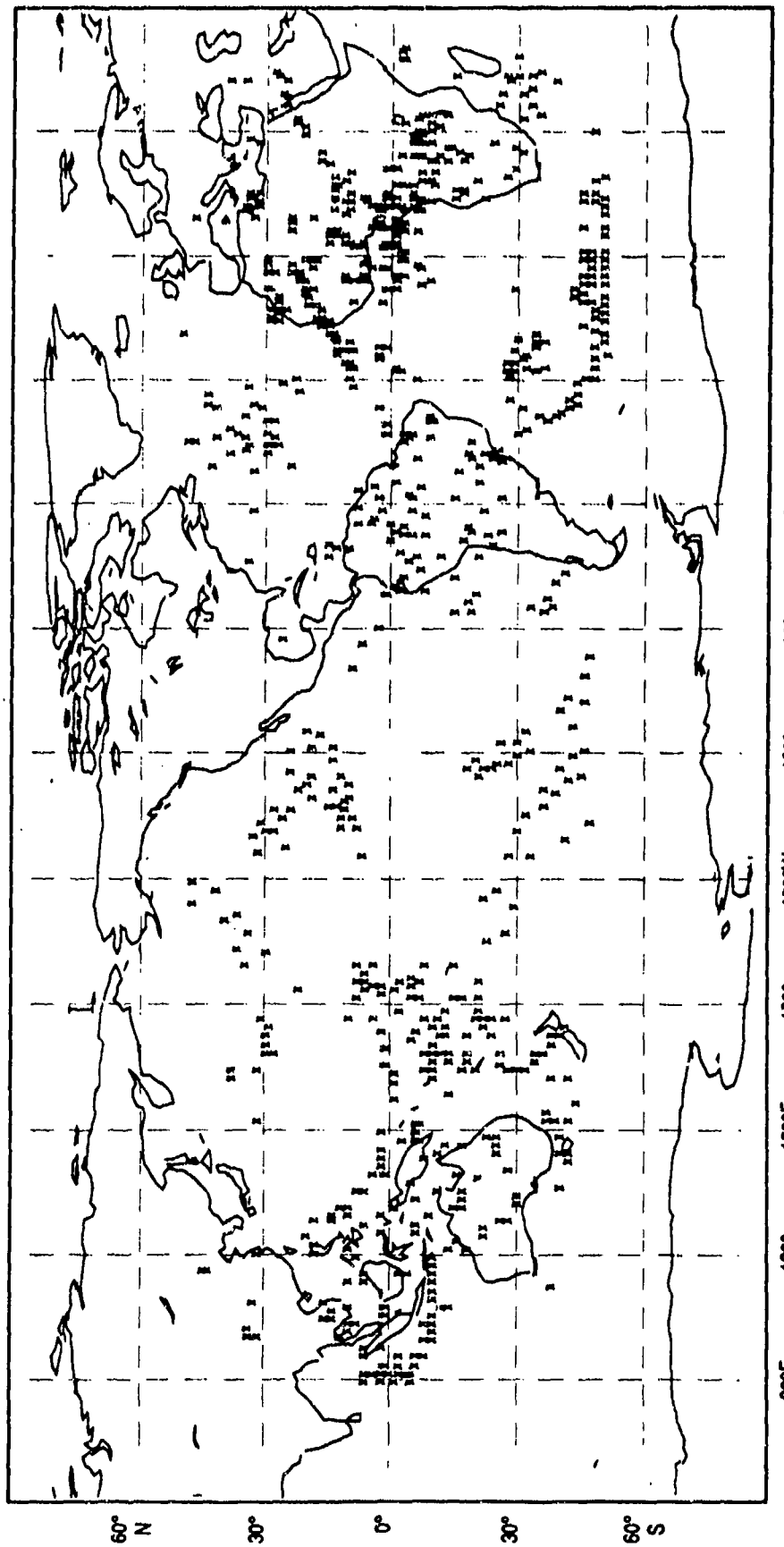

Figure 16. Typical 6-hour availability of cloud-tracked wind observations for all analysis levels.

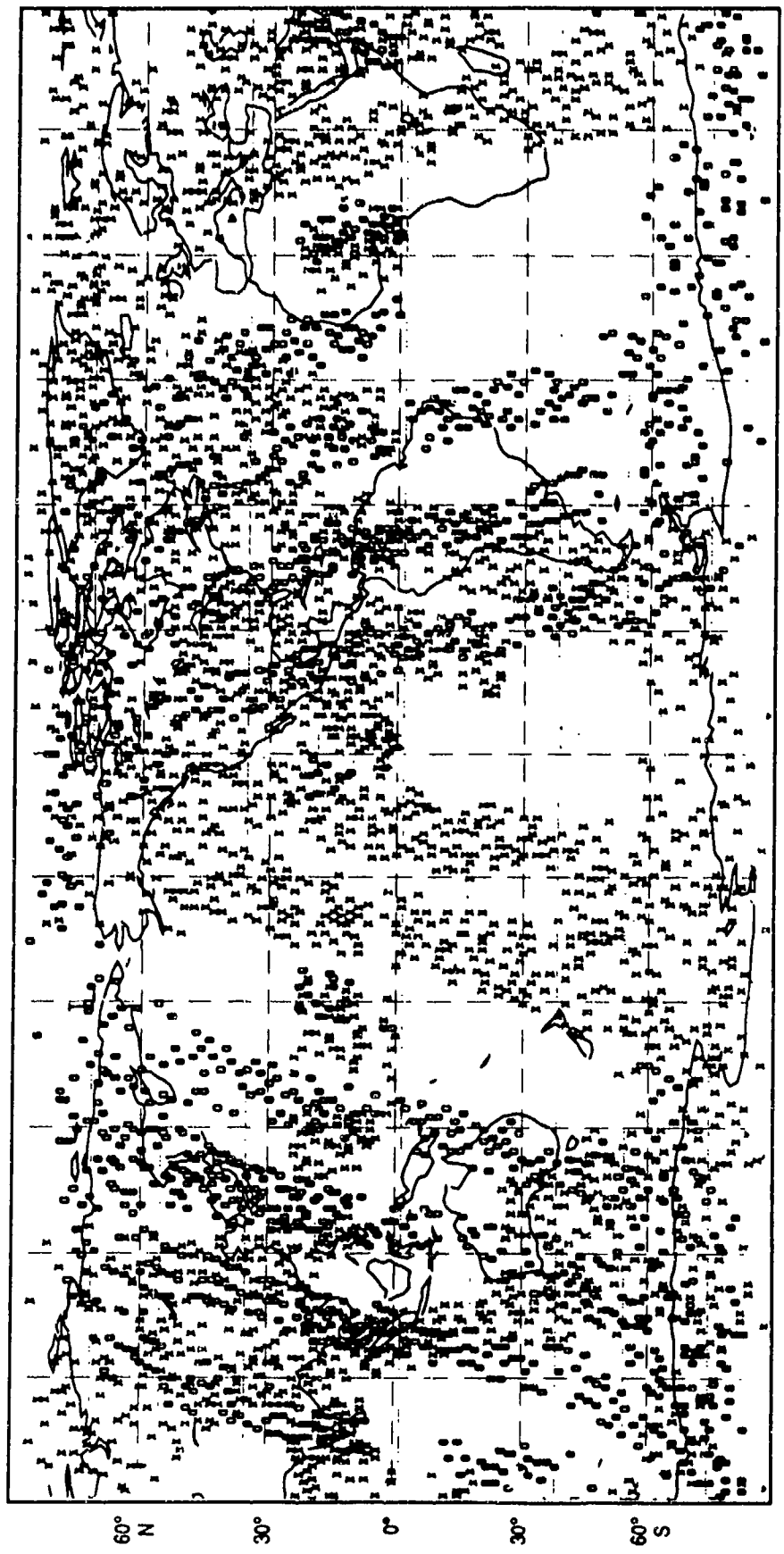

Figure 17. Typical 6-hour coverage provided by the NOAA (X) and DMSP (O) satellite temperature soundings.

reported thickness is positive. The analysis quality flag is set to 0 for all available thickness data; missing or erroneous layers are assigned a quality flag of 99. Lapse-rate checks will also be performed on the satellite soundings; these tests are described in Section 3.3.

Since one of the analysis levels, 925 mb, is not a mandatory pressure level, we compute a 1000–925-mb thickness and a 925–850-mb thickness in a manner consistent with the atmospheric structure reported in the lower layers. The reported 850–700-mb thickness and the 1000–850-mb thickness are used in this calculation. If the lowest layer reported is not bounded by 1000 mb, but the bottom pressure is greater than 925 mb, the calculation is still performed, but only the 925–850-mb layer thickness is computed. First, from the hypsometric equation, we compute the mean temperatures of the two reported layers, which in turn are appropriately weighted to estimate the mean temperature of 925–850-mb layer. Again using the hypsometric equation, the 925–850-mb thickness is computed using the estimated mean temperature of the layer. The 1000–925-mb thickness is then computed by subtracting the 925–850-mb thickness from the 1000–850-mb thickness, when available

Normally, the satellite sounding data are read from the FNOC S0F records, which contain the data received at FNOC from Carswell Air Force Base. These records include layer thicknesses up to 1 mb, where available. However, FNOC also receives sounding data directly from the National Environmental Satellite Data and Information Service in Washington, D.C. These data are stored in the S0G and S0H records, and are in the form of layer mean temperatures up to 50 mb (S0G) and from 50 to 0.4 mb (S0H). If no sounding data are found on the S0F records, the S0G and S0H data are used as alternatives.

The S0G records are processed in much the same way as the S0F records, although the thickness must be computed from the reported layer mean temperature and the pressures bracketing the layer. Mean temperatures from the two lowest layers are used to compute the 1000–925-mb and 925–850-mb thicknesses, as described above. Other layers reported in the S0G records are also incompatible with the layers defined by the analysis levels. Therefore, the available 300–200-mb thickness is decomposed into 300–250-mb and 250–200-mb thicknesses, and the reported 200–100-mb thickness is used to compute 200–150-mb and 150–100-mb thicknesses. The mean temperature in the layer being subdivided is considered along with the mean temperature of the layer below to estimate the mean temperature of the lower of the two new layers. These computations mimic those used for dividing the 1000–850-mb layer, and in each case, the two new layer thicknesses will add up exactly to the original layer thickness.

When the S0F records are missing, the S0H records provide data for the upper layers of the atmosphere. The data are processed in much the same manner as already described—reported mean layer temperatures are used to compute layer thickness in geopotential meters. Only one mismatch occurs between the reported layers and the analysis layers. Thus, the reported 30–10-mb mean layer temperature is used along with the 50–30-mb mean layer temperature to compute the 30–20-mb and 20–10-mb thicknesses. Finally, the thicknesses above 50 mb from

the SOH records must be merged with the soundings from the SOG records. Because of the reduced number of levels reported, there may be twice as many SOH soundings stored as there are SOG. The location of each upper-level sounding is compared to the location of each lower level sounding, and if the latitude and longitude differences are no more than 0.5° each, the data are merged to provide a complete profile of geopotential thickness for all analysis layers, with associated quality flags, thus mimicking exactly the format of the SOF soundings.

3.1.7 SSM/I Wind Speed Data

Estimates of the surface wind speed over the oceans can be derived from measurements made by the Special Sensor Microwave/Imager (SSM/I), a passive microwave radiometer flown on board the DMSP F8 satellite. These observations are derived by taking advantage of the dependency of emissivity on the state of the sea surface (Goodberlet et al., 1990). Currently, FNOC is the only forecast center with operational access to the SSM/I data. Within a 6-hour period, over 200,000 wind speed observations are derived from this sensor at approximately 20-km resolution. Since this data density is far greater than that required by NOGAPS, the high-resolution SSM/I observations are thinned and averaged, resulting in about 2000 observations at 200-km resolution. Figure 18 illustrates the distribution of the thinned SSM/I data available for use by a 1200 UTC analysis. Relatively good global coverage is available over a 24-hour period.

The high-density SSM/I observations are thinned during preprocessing so that only every sixth observation is presented to the analysis. However, even this data density is still much greater than that required for the scales resolved by a global analysis/forecast system. Initially, the analysis may read-in up to 32,000 individual wind speed observations, starting with the current analysis time and working in ±1-hour increments over the 6-hour data window of the analysis. Since the number of original observations within that time window has already been reduced by the preprocessor, sufficient storage is available for the remaining observations. As the analysis processes this data, however, further information consolidation is desirable.

First, the individual wind speed reports are subjected to tests that compare the observed values to the wind speeds produced by the preliminary 1000-mb wind analysis described in Section 5.2. The preliminary field is horizontally interpolated to the location of each observation and the wind speed *increments* are computed as the observed minus the analyzed differences. If the analyzed speed is less than 4 m/sec, but the observed wind speed is more than 3 m/sec *greater* than the preliminary estimate, the SSM/I observation is not saved. Since the wind direction for the SSM/I data will be assigned from this preliminary analysis field, we do not want to use a wind direction from a suspected light and variable wind condition to assign a direction to a stronger observed wind speed. If the analyzed winds are calm, and thus have no direction, we must also reject the SSM/I observation. In situations where the analyzed wind speed is between 4 and 10 m/sec, SSM/I data are rejected only if the absolute value of the increment exceeds 7.5 m/sec. For stronger wind conditions, defined as

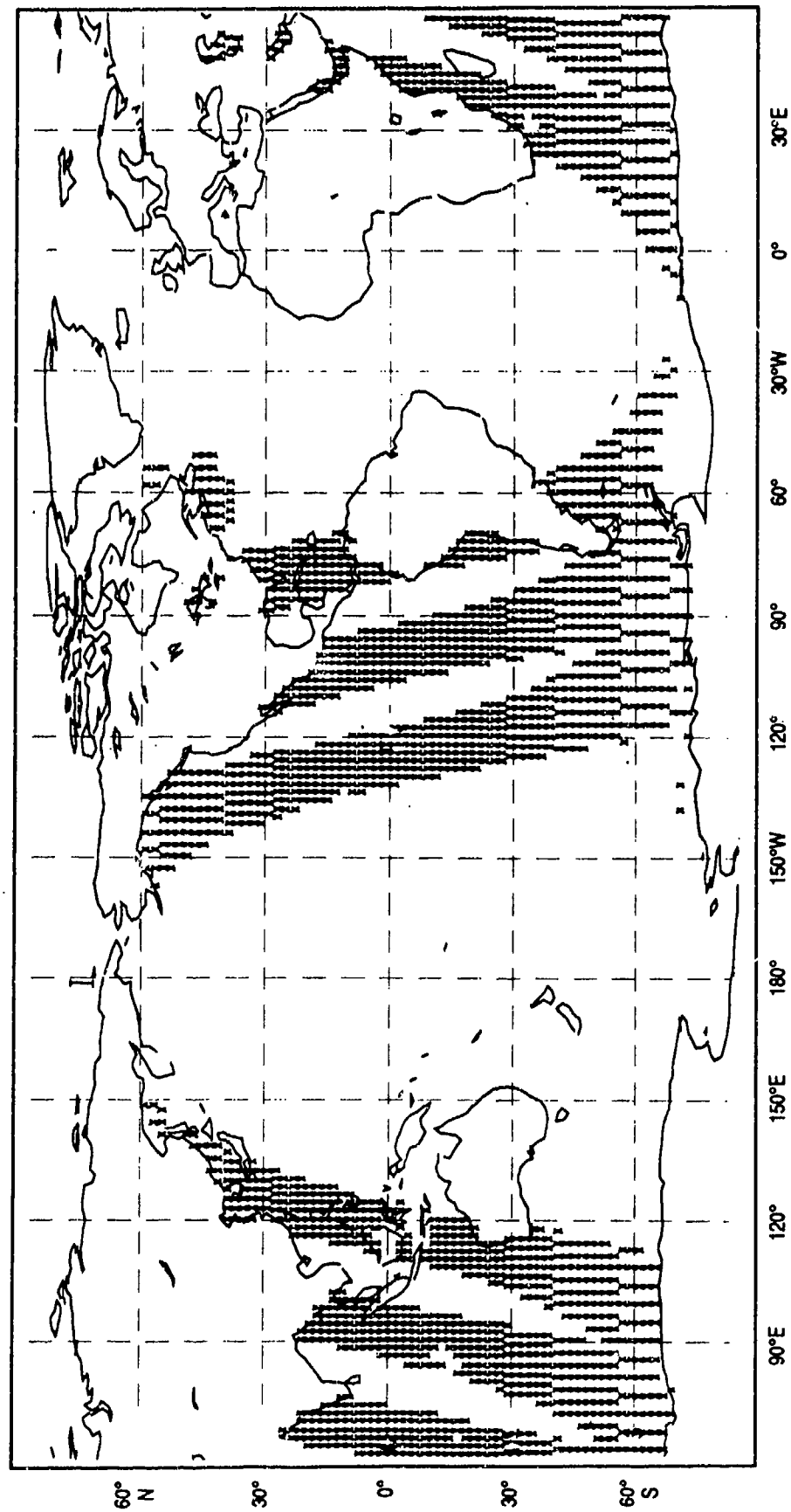

Figure 18. Typical 6-hour coverage provided by the averaged SSM/I wind speed observations.

analyzed speeds in excess of 10 m/sec, an absolute difference of up to 10 m/sec is allowed.

The wind speed increments that pass these quality control checks are binned and averaged to form SSM/I *superob* increments. The *increments*, rather than the full field values, are used to compute the superobs because they are more horizontally homogeneous. Each superob is assigned a latitude and a longitude from the center location of each bin. The bin locations are fixed, with each bin encompassing 2° of latitude and varying degrees of longitude, in such a way that the bins extend over roughly the same physical distance in both the north-south and east-west directions. This layout results in SSM/I superobs with a data density of approximately 200 km. One last caveat is that there must be at least three independent observations in a bin to form a superob. If there are only one or two increments in a bin, they will be ignored.

The final step is to assign a wind direction to each superob wind speed increment. The u- and v-wind components from the preliminary 1000-mb analysis field are horizontally interpolated to the superob locations. From these components, the analyzed wind speed is computed at each location and added to the superob increment to create a full-field wind speed superob. Then, the u- and v-wind components of the superob are computed by multiplying the wind components of the preliminary analysis by the ratio of this superob wind speed to the preliminary analysis wind speed. From this point on, the SSM/I superob components are treated like any other full-field u- and v-wind observations. Any prior processing using the preliminary 1000-mb analysis is ignored. The analysis quality flag associated with each superob wind pair is set to 10, for now.

3.1.8 Synthetic Data

Finally, the global database is supplemented by the creation of synthetic observations for specific applications. The use of synthetic *surface* observations is common practice at the global weather forecast centers. The most commonly used synthetic observations are the subjectively derived estimates of sea-level pressure in the Southern Hemisphere (PAOBS)—observations produced by the Australian Bureau of Meteorology (Guymer, 1978) and provided to the other operational centers. These observations are available at FNOC for the 0000 UTC and 1200 UTC analyses, and their typical distribution is shown in Figure 19. The PAOBS are checked during the preliminary quality control, and are subsequently processed with the other surface data as described.

Locally, FNOC personnel generate synthetic observations of sea-level pressure and surface winds in the vicinity of oceanic extratropical cyclones. Typically, such observations are created in relatively data-sparse areas like the North Pacific, in situations where satellite imagery indicates that the cyclone is deeper than its depiction by NOGAPS. This type of synthetic observation is routinely used in both the 0000 UTC and 1200 UTC analyses (Goerss, 1989). The synthetic observations are bypassed by the preliminary checks. However, these data are stored and processed with the other surface reports and will therefore be subjected to the analysis quality checks.

In June 1990, FNOC also began the assimilation of synthetic wind *soundings* in the vicinity of tropical storms. These soundings are

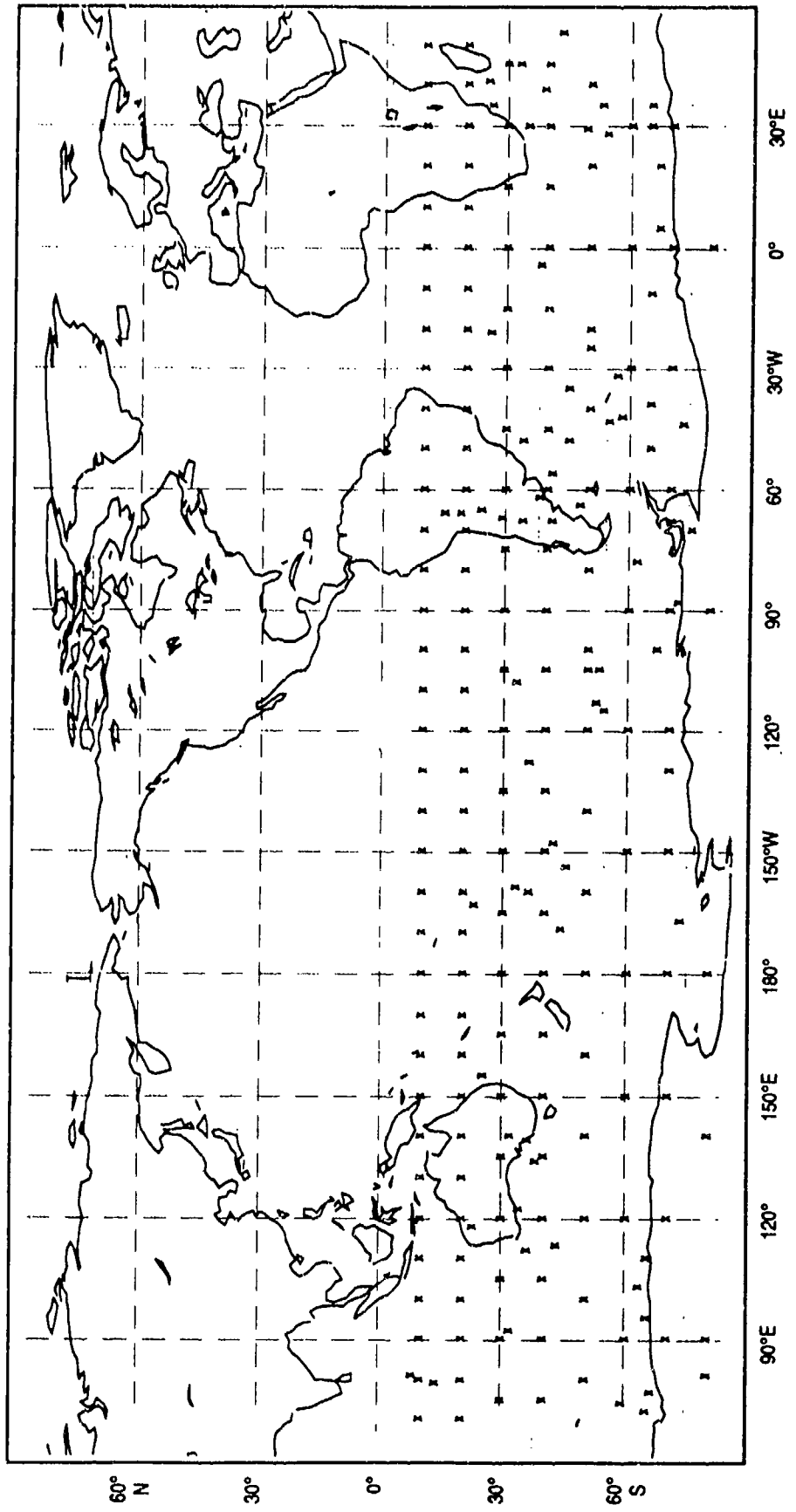

Figure 19. Typical distribution of Australian synthetic surface observations for one analysis time.

automatically generated from the warnings issued by the Joint Typhoon Warning Center (JTWC), Guam, and the National Hurricane Center (NHC), Miami, for tropical cyclones whose maximum wind speeds are 35 kt or greater. The synthetic soundings are centered on the storm's location and reflect the maximum wind speed and radius of maximum wind information contained in the warning message. The preliminary quality checks are bypassed, and the synthetic soundings are subsequently processed by the analysis along with the radiosonde observations.

3.2 Observation Increments

The MVOI is an incremental analysis; that is, it uses information from current observations to update the background fields provided by the forecast model. The *current* observations generally include all data within ±3 hours of the analysis time, although the time window may vary depending upon the particular application of the analysis (Section 5). Once the data within this time window have been processed and converted to observations of geopotential height, geopotential thickness, and u- and v-wind components, they must be transformed into observed increments of the same variables. The procedures used to form the increments are more or less the same for all data types. The 6-hour forecast fields from the NOGAPS spectral model are interpolated to the analysis grid. Franke (1985) showed that significant error can be introduced at this stage in the analysis if simple bilinear interpolation is used. Thus, the appropriate background field is horizontally interpolated to each observation location using a bicubic spline interpolator. If the observation is reported at a defined analysis pressure level, no vertical interpolation is necessary. The observation minus background difference is computed, and the observed value is replaced with the incremental value.

There are a few exceptions to the general procedure: (a) Aircraft and cloud-tracked wind observations are not necessarily at the analysis pressure levels. Thus, the horizontal interpolation of the background field must be done at the levels above and below the off-level observation. The two values at the observation's horizontal location are then vertically interpolated to the level of the observation. The vertical interpolation is linear with respect to pressure. (b) Since thickness is not a model output field, the height background fields are differenced to provide the thickness background fields for each layer. These fields can then be horizontally interpolated to the satellite sounding locations to compute the thickness increments. (c) The marine surface wind components from ships, buoys, and the SSM/I are differenced with the 10-m wind field from the model, valid at the analysis time, rather than the 1000-mb wind field. The 10-m wind field is a NOGAPS by-product that is produced primarily to provide forcing data for the FNOC oceanographic models. The 10-m winds agree more closely with the surface wind reports than do the 1000-mb winds. Then, assuming that the wind *increments* at 10 m are not much different than the increments at 1000 mb, we simply assign these surface wind increments to the first analysis level.

3.3 Analysis Gross-Error Checks

In practice, very few, if any, observations are excluded during the data processing described. The preliminary checks performed on the data

before they are passed to the analysis effectively eliminate or flag the observations with values that are obviously out of range. Similar checks in the analysis are therefore redundant and are performed more as a fail-safe measure than anything else. However, in an operational system, a certain amount of redundancy is desirable, since even a small data glitch can cause an entire system to crash. From experience, we have learned to always expect the unexpected, and we design our systems accordingly.

The remaining analysis quality control algorithms are designed to identify observations that are erroneous even though their values may appear to be perfectly reasonable. These quality tests are therefore performed *after* the observed increments have been computed and always use the absolute difference of the observation from the background. The first quality check made on the increments is the check for gross errors, and only increments that have already been flagged for rejection or increments from the synthetic tropical soundings escape this test. Keeping in mind that the short-range model forecasts have become very accurate, we essentially use the background field as a control on the reasonableness of the data.

The amount of deviation from the background that will be tolerated varies from one data type to another, and is a function of both the observation error $\hat{E}^o$ and the prediction error $\hat{E}^p$ associated with the observation and its location. The appropriate values for $\hat{E}^o$ and $\hat{E}^p$ are estimated using the techniques described in Section 2.2. The observation errors currently assigned to each data type are shown in Table 2. The thickness errors given are for the NOAA retrievals. For DMSP retrievals, these values are multiplied by 1.5 in the northern hemisphere above 70 mb and by 2.0 in the southern hemisphere above 100 mb. Otherwise, the observation errors do not vary from one horizontal location to another.

To perform the gross-error check for each observed increment, we define the quantity T_{il}

$$T_{il} = \left[\left(\hat{E}^p_{il}\right)^2 + \left(\hat{E}^o_{il}\right)^2\right]^{1/2}, \tag{50}$$

where $\hat{E}^p_{il}$ is the prediction error and $\hat{E}^o_{il}$ is the observation error for the increment at location i and level l. Both errors are functions of the level, and the observation error is a function of the data type. While the prediction errors used in the analysis are also a function of horizontal location, these variations have not yet been defined. Thus, the value of $\hat{E}^p_{il}$ used for the gross-error check is allowed to vary vertically but not horizontally. The values used are those shown in Table 3, where the height and thickness errors are derived from the wind errors using equation (48) with a value of the Coriolis parameter valid at 60°.

Larger values of either observation error or prediction error result in larger values of T. Thus, equation (50) implies that data types known to have large errors are given a little more leeway before they are rejected. While this may seem contradictory, it reflects the desire to differentiate between anomalies due to instrument inaccuracy and anomalies that reflect truly erroneous data. Similarly, we also tolerate

Table 2. NOGAPS observation errors.

	Gpt Hgt ϕ (gpm)	U or V Wind (m/sec)				NOAA Thickness (gpm)		
Pres (mb)	Raob	Sounding	Aircraft	Cld-track	Pres (mb)	Clear	Pt Cld	Cloudy
1000	59	2.2	3.0	2.8	1000–925	101	151	151
925	59	2.2	3.0	2.8	925–850	85	123	123
850	59	2.2	3.0	2.8	850–700	167	250	250
700	59	2.2	3.0	3.8	700–500	241	360	360
500	88	2.8	3.0	4.8	500–400	128	192	192
400	98	3.0	3.5	5.8	400–300	165	248	248
300	118	3.2	4.0	6.5	300–250	105	158	158
250	128	3.1	4.0	6.5	250–200	128	192	192
200	137	3.0	4.0	6.5	200–150	165	248	248
150	147	2.8	4.0	6.5	150–100	233	350	350
100	157	2.8	4.0	6.5	100–70	205	308	308
70	167	2.8	4.0	6.5	70–50	193	290	290
50	186	2.8			50–30	293	440	440
30	235	2.8			30–20	233	350	350
20	284	2.8			20–10	398	597	597
10	392	2.8						

	Gpt Height ϕ (gpm)					U or V Wind (m/sec)			
	Land	Ship	D Buoy	F Buoy	PAOB	SSM/I	Ship	D Buoy	F Buoy
Surface	59	59	59	59	236	2.2	2.2	2.2	2.2

Table 3. NOGAPS prediction errors.

These are Values for Data-Rich Areas at 60°				
Pressure (mb)	Wind (m/sec)	GPT Height (gpm)	Pressure (mb)	Thickness (gpm)
1000 mb	2.0	103	1000–925	77
925 mb	2.0	103	925–850	77
850 mb	2.0	103	850–700	110
700 mb	2.3	119	700–500	142
500 mb	2.8	144	500–400	128
400 mb	3.3	170	400–300	141
300 mb	3.8	196	300–250	100
250 mb	3.8	196	250–200	113
200 mb	3.7	191	200–150	136
150 mb	3.7	191	150–100	177
100 mb	3.8	196	100–70	164
70 mb	3.8	196	70–50	157
50 mb	3.8	196	50–30	248
30 mb	5.0	258	30–20	302
20 mb	7.0	361	20–10	562
10 mb	10.0	515		

larger absolute increments in areas with higher prediction errors, reflecting the fact that the background is more likely in error.

To actually perform the error-checking, we specify tolerances that are multiples of T, which define a range of values where the observed increment is considered likely to be erroneous, and a limiting value, beyond which the increment will be rejected. If an increment is accepted as accurate by the gross-error check, it will receive no further checking by the analysis, *unless it was flagged as suspect during the preliminary checks.* Under no circumstances will the analysis quality flag of a questionable observation be reset to indicate that the observation is good. Quality flags can only be changed in the negative sense.

The defined tolerances vary with data type and location and are summarized in Tables 4–6. The most straightforward tests are performed on wind reports (Table 4). Radiosonde, pibal, SSM/I, marine surface, and aircraft wind increment pairs are rejected if either the u- or v-wind increment exceeds 3.5 T, and the wind pair is flagged for further checking if either increment exceeds 2.5 T. The off-level wind reports—aircraft and cloud-tracked winds—are compared to the value of T that is valid at the analysis level at or immediately below the observed pressure. The satellite cloud-tracked wind data are subjected to the most stringent criteria, for they are rejected if either wind increment exceeds 1.5 T. Cloud-tracked winds are either accepted or rejected at this point in the analysis; they are not flagged for further checking.

As an illustration, consider a set of wind observations from various sources, all at one pressure level and with the prediction error the same at each observation location. Since the contribution of the prediction error to T will be constant for all the observations, variations in T will be solely a function of the observation error. Using the appropriate error values for 250-mb wind data from Tables 2 and 3, computed values of T vary from 4.9 m/sec for radiosonde and pibal winds to a high of 7.5 m/sec for cloud-tracked winds. However, since the tolerances are a function not only of T, but also vary with data type, we find that radiosonde and pibal winds will be rejected if either the u- or v-wind observation differs from the background by more than 17.1 m/sec. The comparable limit is 19.3 m/sec for aircraft winds, and only 11.3 m/sec for cloud-tracked winds. With the exception, perhaps, of the cloud-tracked

Table 4. Gross-error check wind tolerances.

T Varies with Level and Data Type			
Data Increment Type	No Checking	Further Checking	Rejection
Aircraft Wind	<2.5 T	2.5–3.5 T	>3.5 T
SSM/I Wind	<2.5 T	2.5–3.5 T	>3.5 T
Ship/Buoy Wind	<2.5 T	2.5–3.5 T	>3.5 T
Radiosonde Wind	<2.5 T	2.5–3.5 T	>3.5 T
Pibal Wind	<2.5 T	2.5–3.5 T	>3.5 T
Cloud-Track Wind	≤1.5 T	None	>1.5 T

winds, rather large deviations from the background are still accepted by the gross-error check, by design. Absolute increments smaller than 12.2 m/sec for radiosondes and pibals, 13.8 m/sec for aircraft, and 11.3 m/sec for cloud-tracked winds will be accepted as is, unless they were flagged as suspect during the preliminary checks. Values in between will be subjected to comparisons with surrounding observations later in the analysis.

The tolerances specified for conventional radiosonde and surface height observations are more variable, since they are adjusted according to the latitude of the observation (Table 5). Surface height increments are flagged for additional checking if their absolute value exceeds 3.0 T', where $T' = 0.8\,T$ for observations between −30° and 30°N and $T' = T$ elsewhere. Similarly, increments exceeding 5.0 T' are rejected, but only if they are over land or between −25° and 25°N. Marine height observations in the midlatitudes and polar regions cannot be rejected by the gross-error checks. However, they can be flagged for additional checking. The PAOBS are processed along with the surface data, but the tolerances

Table 5. Gross-error check height tolerances.

T Varies with Level and Data Type			
Data Increment Type	No Checking	Further Checking	Rejection
Land Surface Height			
Extra-Tropics	<3.0 T	3.0–5.0 T	>5.0 T
Tropics	<2.4 T	2.4–4.0 T	>4.0 T
Marine Surface Height			
Extra-Tropics	<3.0 T	≥3.0 T	None
Tropics	<2.4 T	2.4–4.0 T	>4.0 T
Australian PAOB Height			
Extra-Tropics	<6.0 T	≥6.0 T	None
Tropics	<4.8 T	4.8–8.0 T	>8.0 T
Radiosonde Height			
Polar Areas			
Below 30 mb	<4.8 T	4.8–8.0 T	>8.0 T
30 to 20 mb	<7.7 T	7.7–12.8 T	>12.8 T
10 mb	<11.5 T	11.5–19.2 T	>19.2 T
Midlatitudes			
Below 30 mb	<3.0 T	3.0–5.0 T	>5.0 T
30 to 20 mb	<4.8 T	4.8–8.0 T	>8.0 T
10 mb	<7.2 T	7.2–12.0 T	>12.0 T
Tropics			
Below 30 mb	<2.4 T	2.4–4.0 T	>4.0 T
30 to 20 mb	<3.8 T	3.8–6.4 T	>6.4 T
10 mb	<5.8 T	5.8–9.6 T	>9.6 T
Synthetic Radiosonde			
Midlatitudes			
Below 30 mb	<3.0 T	3.0–5.0 T	>5.0 T
30 to 20 mb	<4.8 T	4.8–8.0 T	>8.0 T
10 mb	<7.2 T	7.2–12.0 T	>12.0 T
Tropics	All	None	None

are increased by a multiple of 2 for these synthetic observations, thus allowing larger increments to pass the gross-error check.

The rejection and checking tolerances for radiosonde height data are equal to 5.0 T" and 3.0 T'', respectively. Several factors are considered in defining T''. First we define T' as a function of latitude, with $T' = 0.8\ T$ between latitudes –30° and 30°, $T' = T$, and $T' = 1.6\ T$ poleward of latitudes –60° and 60°. Thus, observations in the polar regions are given more leeway than those in the mid-latitudes and tropics, thereby accounting for the increased magnitude of the background errors in the polar areas. Then, T'' is used to allow further variations of the tolerances with height, over and above the variations induced by the observation and prediction errors. This increase in tolerance is applied only at 30 mb and above, with $T'' = 1.6\ T'$ at 30–20 mb and $T'' = 2.4\ T'$ at 10 mb, the uppermost analysis level. This final increase was introduced to control the occasional event where the spectral forecast model displays especially large errors at the upper levels. In these cases we do not want radiosonde data to be rejected. We have found that being overly tolerant of the data at these levels does no harm.

Even though our theoretical development of the MVOI assumes that observation errors are uncorrelated, in reality, observation errors for satellite thickness increments tend to be highly correlated horizontally, especially for observations from the same satellite. Because of this correlation, erroneous observations would lend support to each other when subjected to the corroboration check by the analysis. Therefore, more stringent rejection tolerances are used for the gross-error check of thickness data, with no provision for further checking by the analysis (Table 6). The rejection tolerance is set at 1.5 T''. The variation with latitude, defined by T', is exactly the same as for the radiosondes. Additional variations with height are defined for the layers above 50 mb, with $T'' = 1.6\ T'$ for the 50–30-mb and 30–20-mb layers and $T'' = 2.4\ T'$ for the 20–10-mb layer. After these initial checks are made,

Table 6. Gross-error check thickness tolerances.

T Varies with Level and Data Type			
Data Increment Type	No Checking	Further Checking	Rejection
Satellite Thickness			
Polar Areas			
Below 50 mb	≤2.4 T	None	>2.4 T
50 to 20 mb	≤3.8 T	None	>3.8 T
20 to 10 mb	≤5.8 T	None	>5.8 T
Extra-Tropics			
Below 50 mb	≤1.5 T	None	>1.5 T
50 to 20 mb	≤2.4 T	None	>2.4 T
20 to 10 mb	≤3.6 T	None	>3.6 T
Tropics			
Below 50 mb	≤1.2 T	None	>1.2 T
50 to 20 mb	≤1.9 T	None	>1.9 T
20 to 10 mb	≤2.9 T	None	>2.9 T

the satellite sounding data that are not rejected are then subjected to lapse-rate checks.

Lapse-rate checks are required because of the inherently poor vertical resolution of the derived measurements, which results in satellite retrieval thickness errors in the lower troposphere that are often negatively correlated with errors in the upper troposphere. In situations where the actual atmosphere is unstable (temperature decreasing more rapidly with height than normal), the satellite soundings tend to be too stable. The opposite is true in stable atmospheric conditions. In either case, the vertical temperature structure of the atmosphere is almost always depicted more accurately by the analysis background. We have found that in the more extreme situations the absolute difference between the lower tropospheric thickness increments and those from the upper troposphere is large. The lapse-rate checks are designed to identify those cases where the use of the satellite soundings would impact negatively upon the analysis and the ensuing model forecast.

The lapse-rate checks are only performed for soundings where the 1000–925-mb thickness is available, thereby disregarding many of the soundings over land. The total thickness increments for 1000–700 mb and 500–300 mb are computed by summing the reported intermediate layers. Allowing for the fact that the 1000–700-mb layer represents approximately 1.43 times the mass of the 500–300-mb layer, the lower layer is multiplied by 1.43 before the upper layer value is subtracted from it. The allowed tolerance for this difference is estimated by summing the thickness prediction errors for the three layers from 1000 to 700 mb, multiplying by 0.58 and adding this result to the thickness prediction errors for the two layers from 500 to 300 mb. Using the values shown in Table 3, this results in a tolerance of 422 gpm. This intermediate value is multiplied by 1.333 to get the absolute difference of 563 gpm. Any sounding whose difference exceeds this value has the lowest six layers of the sounding (essentially the tropospheric part) rejected. For soundings with differences between 422 and 563 gpm, the tropospheric part of every other sounding is rejected. The lapse-rate check does not affect any portion of the sounding above 300 mb. It is possible to adjust the multiplicative factors of 0.58 and 1.333 through the executable job stream, thus requiring no software changes.

Table 7 illustrates the typical number of observations flagged as either suspicious or bad by the preliminary checks and the analysis gross-error check. The largest rejection rates are associated with satellite wind and sounding data, consistent with the fact that these observations receive no further checking by the analysis. The following numbers are all approximate, but typically 15–20% of the cloud-tracked winds are rejected by the gross-error check. About 7% of the thickness observations are rejected between both the gross-error and lapse-rate checks. For the other data types, the number of individual observations rejected by the gross-error check is very small. Only 1% of the surface reports and less than 2% of the radiosonde observations are considered erroneous; these numbers hold true for both wind and height data. Wind reports from pibals and from aircraft are rejected at the rate of 4–5%. The number of questionable observations is only slightly larger. About 3% of the conventional surface and radiosonde wind and height reports are

Table 7. Quality control results.

Following Preliminary Checks and Analysis Gross-Error Checks		
Data Increment Type	Percent Rejected	Percent Suspected
Aircraft Wind	4-5%	4-5%
Pibal Wind	4-5%	8%
Radiosonde Wind	2%	3%
Cloud-Tracked Wind	15-20%	0%
Marine Surface Wind	1%	3%
Radiosonde Height	2%	3%
Surface Height	1%	3%
Satellite Thickness	7%	0%

flagged for further checking. Aircraft wind observations undergo further scrutiny about 4–5% of the time, and pibal winds are considered suspect in about 8% of the cases.

In practice, no observation is ever removed from the data set. Instead, the analysis quality flag is reset, as necessary, to indicate those increments that have been rejected and the values that are still suspicious. The analysis will then ignore the data with rejection flags, and the questionable values will be subjected to yet another quality check within the analysis to determine if they are consistent with other nearby increments (Section 4.4). Increments that pass both the preliminary quality checks and the gross-error checks will undergo no further quality control and will influence the outcome of the analysis at surrounding grid points. The analysis quality flags are output along with the original observations and saved in the global database, which allows us to monitor the performance of individual platforms, countries, and data types for routinely large biases or errors.

4.0 Analysis Process

While Section 2.0 emphasized the specification of the statistical parameters for the MVOI, it is obvious from equation (1) that the analyzed increment at a point k is also determined by the particular set of observations that are used to form the summation on the right-side of that equation. To optimize the selection of the observations, the Navy's MVOI analysis scheme has been patterned after the volume method introduced by Lorenc (1981). The major advantage of the volume method is that it permits the production of optimum interpolation analyses at a large number of grid points from one set of observations, so that the necessary matrix and vector calculations need only be performed once. This increased efficiency allows the use of many more observations for each analysis point than is computationally feasible with the grid-point method (DiMego, 1988). Furthermore, it simplifies the data selection process and allows for rigorous quality control of the observation increments.

4.1 Analysis Volumes

One of the most important considerations in the design of the volume method for the MVOI is the selection of the analysis volumes themselves.

By our definition, a volume represents not only a set of grid points, but also the physical space containing the set of observations that will influence the analysis at these grid points. Due to software constraints, the number of observations within any given volume cannot exceed some specified maximum. Thus, to ensure a sufficient set of observations within each volume, it is desirable to have the volume size vary with data density. Fortunately, the distribution of data around the globe is fairly constant in time, which allows us to specify the volume sizes in some predetermined fashion.

First, the globe is divided into a set of 838 overlapping volumes that vary in horizontal extent (Fig. 20), but are fixed in vertical extent. Each volume contains all 16 analysis pressure levels, thus entirely eliminating the need for vertical averaging. The polar caps comprise two of the volumes and, due to the convergence of the meridians, account for a disproportionate number of grid points with respect to the actual physical areas they encompass. The polar cap volumes are chosen to be as large as possible, given the typical distribution of observations in each region. The south polar cap extends to 79.9°S while the north polar cap extends to 81.4°N. Thus, over 10% of the global analysis grid points are contained in these two volumes.

Over the remainder of the globe, the analysis volumes are arranged in overlapping latitudinal strips. The north-south extent of these strips is 18° in the Southern Hemisphere and 9° in the Northern Hemisphere, and each strip overlaps one-half of the adjacent strips to the north and south of it. Within each strip, the longitudinal extent of each volume is varied so that the east-west distance covered by a volume is less in areas rich in conventional data than in areas sparsely covered by conventional data (generally over the oceans). The volumes within each strip also overlap one another, with each volume extending from the center of the volume west of it to the center of the volume east of it. Thus, with the exception of the polar caps, each grid point is included within four separate volumes, resulting in four separate estimates for the analyzed increment at each point. The final result at each point is obtained by computing the appropriate weighted sums of the various analyzed increments at the point. The overlapping volumes and the resulting averaging process for the analyzed increments prevent the introduction of any false gradients or discontinuities at the volume boundaries.

4.2 Data Selection

Since all ϕ, u, v, and $\Delta\phi$ observations within a volume are used to estimate the analyzed ϕ, u, and v increments at each grid point in the volume, it is also very important to ensure the proper distribution of observations within each analysis volume. A representative number of observations at each analysis level is desirable, as well as a reasonable horizontal distribution, with an appropriate mixture of mass and wind observations. First priority is given to conventional radiosonde, pibal, and surface observations, followed by SSM/I winds, satellite temperature soundings, aircraft, and cloud-tracked winds, in that order. Satellite thicknesses are used only above 500 mb for volumes rich in conventional data, while in areas especially rich in conventional data, thicknesses are included only above 200 mb.

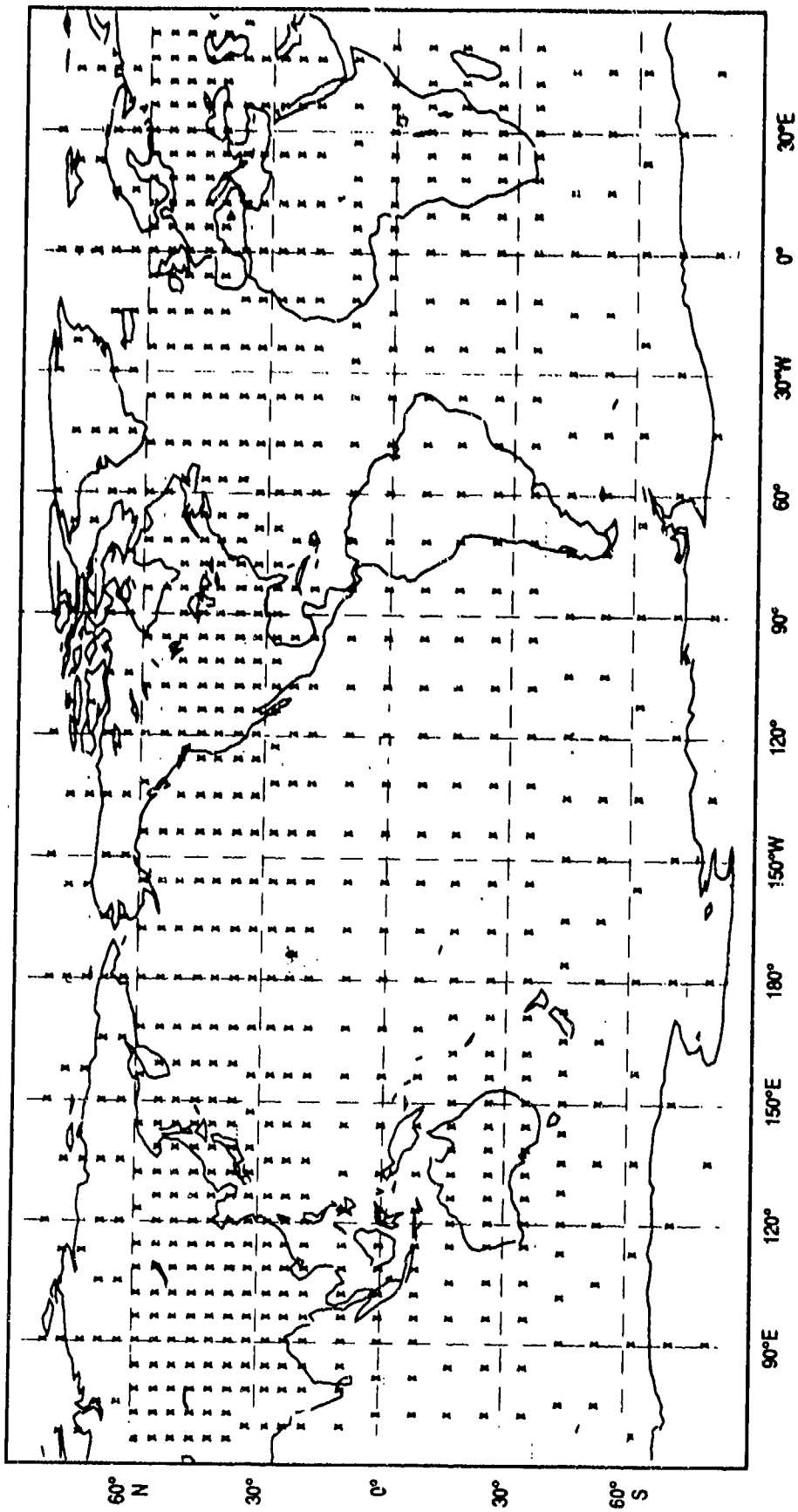

Figure 20. Locations of the grid volume centers used in the NOGAPS MVOI analysis.

The total number of observations allowed for each volume (counting ϕ, u, v, and $\Delta\phi$ separately) cannot exceed 360, and typically averages around 300. However, the areal extent of the volume is symmetrically expanded if the total number of observations found is less than 60, but only for the purpose of including more observations. The analysis itself is still performed only for the grid points contained within the original volume. A maximum of two expansions is permitted, with each expansion increasing the east-west and north-south extent of the volume by 50% of the original distances. For example, an original volume that was 1000 km on a side could be expanded to as large as 2000 km on a side. Typically, volume expansion is only required when normal amounts of data are not received prior to the analysis.

All data types are sorted by latitude and scanned in order of their priority to find the observations in each analysis volume. To ensure the proper mix of data types, limits are imposed on the number of observations of each type that can be included in a given volume (Table 8). The data collection process begins with the first observation in a set, and proceeds to gather every nth observation, where n ranges from 1 to 5 based on the observational density of the data type. The same procedure is followed again, this time beginning with the second observation and selecting every nth observation. These iterations continue until all the observations of one data type in the given volume have been collected, or until the limit for that data type is reached. We then proceed to the next data type, and repeat the process. Because of the prior sorting, this iterative collection procedure ensures that each data type will be uniformly distributed throughout the volume.

As Table 8 illustrates, we still rely heavily on the radiosonde data when it is available. Since there are so few pibal soundings in any given volume, it is not necessary to place any restrictions on their number; all of them are included. The number of thickness observations from satellites will be reduced from 252 to 126 in volumes where other sounding data are plentiful. This reduction is consistent with the fact that we ignore the lower-level portion of the satellite soundings in areas rich in conventional data, typically over land. Over the oceans, the 252 observation limit on the thicknesses ensures that space is available for aircraft and cloud-tracked wind observations.

4.3 Determination of the Weights

Once the N-observed increments for a volume have been collected, the weights must be computed for each increment relative to each grid point in the volume. Recall from the earlier discussion that the weight w_{ik} is dependent upon three statistical quantities—the observation error, the prediction error, and the prediction error correlations, where the correlations are computed between the observation location i and the locations of the other $N-1$ observations in the volume, and between

Table 8. Observation limits per volume.

Counts Include Each Individual ϕ, u, v, and $\Delta\phi$							
Total	Radiosonde	Pibal	Surface	SSM/I	Sat. Thickness	Aircraft	Sat. Wind
360	270	—	28	24	252	36	24

the N observation locations and the grid location k. Except for the correlations between observation and grid locations, these quantities can be computed once and used for all grid locations in the volume. This feature of the volume method makes the use of a large number of observations for the analysis at each grid location computationally feasible. Most of the computations involved in determining the values of the weights are involved in inverting the $N \times N$ matrix $\mathbf{M}$ for evaluating equation (21). In the NOGAPS MVOI, there are over 460,000 grid locations contained in just over 800 volumes. Thus, the grid-point method would require over 500 times the number of matrix inversions that are required for the volume method. Since the number of computations required for a matrix inversion is on the order of N^2, the volume method permits the use of more than 20 times as many observations for each grid location without increasing the computation time.

In our previous discussions of prediction errors (Sections 2.2 and 3.3), the relationship between the height and wind component errors described by equation (48) assumed a constant value for the Coriolis parameter $\mathcal{F}$. For example, the values in Table 3 are computed using the value of $\mathcal{F}$ at 60°N and are used for the gross-error check, while the illustration in Figure 3 is based on the value of $\mathcal{F}$ at 45°. However, within the analysis, the prediction errors are varied with horizontal location. For each volume, the average value of the Coriolis parameter within the volume is determined, with the caveat that the absolute value of the average Coriolis parameter is never permitted to be less than its absolute value at 30°. For volumes rich in conventional data, the wind component prediction errors are those displayed in Table 3. For data-sparse volumes, the prediction errors for the wind components are increased by a factor of 1.3. The height prediction errors for a volume are then computed from the wind prediction errors using equation (48).

Even though all observed increments in the volume contribute to the analysis at grid-point k, the weights computed for some increments will be larger than others, with some increments having little influence on the actual outcome at point k. However, the same increments may have a much larger impact on the analyzed increment at some other point in the volume. To further illuminate how the optimum interpolation technique works, we will discuss how the different statistical quantities affect the actual weight received by the various observations relative to the analysis at a particular point.

First, consider the effect of the normalized observation error (the ratio of observation error to prediction error). If two observed increments are co-located, the prediction error is the same, so the increment with the largest observation error would receive the smaller weight. Thus, if provided data from many sources, the MVOI would give more weight to observation types known to be the most reliable. Furthermore, if the prediction error is large compared to the observation error, the analysis will draw more closely to the observations. However, if the observation error is large compared to the prediction error, the analyzed increments will be smaller and the resulting analysis will more closely resemble the background field.

Second, consider the effect of the prediction error correlation between the observation location and the grid-point location. Since the

height-height prediction error correlation model is a function of distance, in general, height and thickness observations that are farther from the grid point (in three-dimensional space) receive less weight for the analysis of height at the grid location. However, for other data combinations, the correlation functions are not circular (Figs. 6b–f). For example, the functions correlating height and wind data are lobed, while the $\langle uu \rangle$ and $\langle vv \rangle$ functions are somewhat elliptical. Thus, for an analysis of u at a grid point, the u-wind observations east and west of the grid point receive more weight than those sampled in the cross-component direction. For an analysis of ϕ at a grid point, the v-wind increments to the east-west and the u-wind increments to the north-south have the most influence. Given the known relationship between the height gradient and the u- and v-wind components, such structures make sense physically. In the tropics, the geostrophic constraint is relaxed, as evidenced by the decreased correlation between the height and wind fields shown in Figures 7b and c. Increasing the divergence allowed in the wind field decreases the coupling between the u and v components (Fig. 7d), while only slightly changing the shape of the $\langle uu \rangle$ and $\langle vv \rangle$ functions (Figs. 7e–f).

The final parameter influencing the weight w_{ik} is the set of prediction error correlations of the observation locations with the other data locations in the volume. Whereas the previous discussion accounted for the distribution of the observations relative to the grid-point location, the prediction error correlations between observation locations account for the distribution of the observations relative to one another. The effect of these terms is to essentially downweight clusters of observations, particularly those of the same variable type. For example, consider two height observations equidistant from a grid point but on opposite sides. All other properties being equal, the two observations would receive equal weights. However, if the two observations were located on the same side of the grid point, still at the same distance, they would receive less weight than in the first case, since now the prediction error correlation of the two observation locations is higher (Clancy et al., 1989).

While considering the contributions of the various terms in isolation is educational, in reality, the weight a particular increment receives results from a complex interaction of all these factors. However, it is apparent that, unlike earlier objective analysis schemes that essentially averaged the nearby data, an optimum interpolation analysis scheme makes some very intelligent decisions about how to treat the various, often conflicting, sources of information it has available.

4.4 Analysis Quality Control

As the analysis estimates are made at each grid location, the analysis performs further quality-control checks on increments that were flagged earlier as suspect by either the data preprocessor or by the analysis gross-error checks. This phase of the quality control attempts to verify that the questionable values are supported by the other observed increments. To accomplish this task, each flagged increment is compared to an analyzed increment computed at the *observation* location with the flagged increment in question excluded. If these two values differ by more than the estimated interpolation error for that location, the increment

is flagged for rejection, and it is permanently removed from any further consideration by the analysis.

To perform this final stage of quality control, we first define the expected interpolation error at the location of a flagged observation to be the ensemble average $\left\langle \left(\tilde{f}_i^a - f_i^o \right)^2 \right\rangle$. The estimate of the interpolation error is a function of the observation error $\left(\varepsilon_i^o \right)^2$, and after some manipulation (Lorenc, 1981), it can be shown that

$$\left\langle \left(\tilde{f}_i^a - f_i^o \right)^2 \right\rangle = \left(\varepsilon_i^o \right)^2 + 1 - \sum_{j=1}^{N} \tilde{w}_j m_{ij} , \tag{51}$$

where $\tilde{w}_j$ are the weights w_j computed for each observation in the volume, modified in such a way that none of the flagged observations in the volume have any influence on the estimate. The m_{ij} are elements of the column of matrix **M** that is associated with the observation i. The derivation of the interpolation error estimate assumes that all the other estimated errors and correlations used are perfect. Since this is obviously not the case, we arbitrarily add 0.1 to the interpolation error estimate to account for these other sources of error.

Once we have estimated the interpolation error at each flagged observation location from the right-hand side of equation (51), we compute the analyzed increments, the $\tilde{f}_i^a$, at the same locations, again not allowing any of the potentially bad observations to influence the calculation. The questionable increments are subtracted from these analyzed increments, and the analysis/observation deviations $\left(\tilde{f}_i^a - f_i^o \right)^2$ are compared to the expected interpolation errors at the same locations. The differences between the computed and expected values are used to sort the flagged observations so that the observations with the largest differences from the expected errors will be checked first by the analysis.

Proceeding in this sorted order, each flagged observation is individually checked against a prescribed tolerance, given by

$$TOL = T_0^2 \left[\left\langle \left(\tilde{f}_i^a - f_i^o \right)^2 \right\rangle \right] + 0.1 \tag{52}$$

where T_0^2 is currently 10. The analysis/observation deviation is compared to this tolerance, and if $\left(\tilde{f}_i^a - f_i^o \right)^2 > TOL$, the observation is rejected. For this purpose, the computations of the interpolation error estimate and the analyzed value at the location of the suspected data do *not* include the influence of the observation being tested, but *do* include the other flagged observations in the volume. However, once an observation has been rejected, it is not allowed to influence the decisions made about any other observations, thereby explaining why the observations are sorted so those most likely in error are checked first. Once every questionable increment has been subjected to this final corroboration test, the weights of the remaining good observations are recomputed before the analyzed increments are determined for each grid point in the volume. Lorenc (1981) describes how to perform these computations efficiently.

The number of observations rejected during this stage of the analysis cannot exceed the percentage of observations that were flagged for further checking by the previous quality-control algorithms. Of course, not all of the flagged observations will be rejected, since some of them are undoubtedly supported by other nearby observations. When corroborated by other data, the observed increment should not differ from the analyzed estimate at the observation location by more than the allowed tolerance. Since the volumes overlap one another, however, it is possible for an observation to be included in the analysis within one volume, only to be rejected later when it checked against a different set of data. While this inconsistency is not really desirable, the alternative—essentially doing the analysis twice—is too time-consuming to be practical, given current computer resources.

5.0 Analysis Applications

The software developed to perform the global analysis described in the previous section was designed so that, with minimal modification, it could be utilized to satisfy many atmospheric analysis requirements at FNOC. In this section we will describe these different applications and the software modifications that are made to the analysis for each case.

5.1 NOGAPS

Daily operations at FNOC are divided into two watches, each beginning 1 to 2 hours after the synoptic hour. NOGAPS 3-day and 5-day forecasts are produced each day at 1200 UTC and 0000 UTC, respectively, using all of the data available at 3 hours past the synoptic hour (+3 hours). We refer to these products as the real-time run, for they are the products distributed operationally. As previously mentioned, NOGAPS is run with a 6-hour data assimilation cycle, which allows the inclusion of observations that are not available for the initial real-time run. Thus, a reanalysis (post-time analysis) for 0000 UTC or 1200 UTC is performed using all data available at +8 hours. A 6-hour model forecast is made from the post-time analysis and used as the background for the 0600 UTC or 1800 UTC (off-time) analysis, which is performed using all data available at +10 hours. Then, a 6-hour model forecast is made from the off-time analysis to be used as the background for the next synoptic hour, for both the real-time and the post-time runs.

5.2 Preliminary Analysis

Prior to each real-time run of NOGAPS, a global low-level analysis is run using all data available at +2 hours. During this run, the MVOI analysis described in Section 4 is performed at the four pressure levels from 1000 mb to 700 mb, inclusive. All data types are used for this analysis except for aircraft reports, satellite-derived temperature soundings, and SSM/I surface wind speeds. This analysis is used by FNOC personnel to determine areas where synthetic surface observations should be generated and entered into the NOGAPS data base prior to the real-time run. It is also used to provide wind directions for the SSM/I wind speed observations prior to their ingest into the real-time NOGAPS analysis.

5.3 Limited-Area Analyses

The NOGAPS analysis has also been modified so that, if desired, the analysis can be performed only for volumes covering a specified area, but still using the background field from the global forecast model. This limited-area analysis requires only a small fraction of the time that it takes to run the full global analysis, and it is used as a tool by the FNOC personnel responsible for the generation of synthetic surface observations in the vicinity of extratropical cyclones. Prior to admitting these observations into the operational database, the limited-area analysis is run to ensure that the observations they have created will have the desired effect upon the NOGAPS analysis. Since the analysis at any grid point is independent of the results at any other grid point, given the same database, the limited-area analysis can exactly duplicate the global MVOI in a selected region.

5.4 NORAPS

To provide higher resolution, more localized information, the Navy Operational Regional Atmospheric Prediction System (NORAPS) is run for four different areas each watch. The regional analyses differ from the limited-area analyses, since NORAPS is a complete data assimilation system that cycles with its own analysis and forecast model. The NORAPS forecast model is a relocatable grid-point model (Hodur, 1987), which is run with 100-km resolution for the Western Atlantic and Western Pacific areas, with 80-km resolution for the Mediterranean area, and with 40-km resolution for the Persian Gulf area. For each area, the MVOI analysis fields are produced on the forecast grid of the model at the same 16 pressure levels used by the global analysis. The analysis background fields are 12-hour forecasts valid at the analysis time made by the NORAPS forecast model. The observational data base and data selection strategy is the same as that used by the global analysis. Since NORAPS has been designed so that it can be located anywhere in the world, the variable-size volumes, such as those used in NOGAPS, are not practical. Thus, the areal extent of each NORAPS analysis volume is an approximately 1200-km square that is permitted to expand if it does not contain a minimum of 60 observations. The maximum number of observations allowed in a NORAPS volume is 300.

5.5 Stratospheric Analysis

To further satisfy Navy requirements, FNOC produces a stratospheric analysis each day for 0000 UTC and 1200 UTC. The differences between this analysis and the NOGAPS analysis are outlined here. The stratospheric analysis is performed on a $2.5° \times 2.5°$ spherical grid for twelve pressure levels from 200 mb to 0.4 mb. The analysis levels are the standard pressure levels from 200 mb to 10 mb, inclusive, along with 5 mb, 2 mb, 1 mb, and 0.4 mb. The background fields utilized by the stratospheric analysis are the same as those used by the NOGAPS analysis for levels up to 10 mb. For the levels above 10 mb, the background fields are the fields from the previous analysis (12-hour prior) adjusted by the difference between the 10-mb background fields and the 10-mb fields from the previous analysis. That is, we assume that the magnitudes of the analyzed ϕ, u, and v corrections are constant with height above 10 mb at a given location, and adjust the background fields accordingly before performing the next analysis. The prediction error estimates for these upper levels

are increased considerably to reflect the fact that these fields are not as accurate as the model-controlled background fields. Thus, the resulting analyses at the upper levels are more greatly influenced by the observational data than by the background fields.

The only types of observations used in the stratospheric analysis are radiosondes and satellite-derived temperature soundings. Virtually the only data available at levels above 10 mb are the thickness observations derived from the two NOAA polar-orbiting satellites. To improve the data coverage for the analysis, satellite observations are utilized for a 12-hour time window beginning 9 hours before the analysis time. The radiosondes used are those valid at the analysis time. Since the global distribution of data above 200 mb is relatively uniform, there is no need for the data-dependent analysis volume scheme described in the previous section for the NOGAPS analysis. Thus, for the stratospheric analysis, the areal extent of each volume, excluding the polar caps, is approximately a 2000-km square.

5.6 Shipboard Analyses

The MVOI analysis has also been adapted for shipboard use on the Tactical Environmental Support System (TESS(3)). This new hardware will allow ships at sea to receive and process observations, satellite imagery, and FNOC environmental products. The sensor package accompanying TESS(3) gives ships the capability to automatically sample and process their own observations. With resident applications programs, such as the MVOI, information from these various sources can be combined to produce updated, localized analyses in support of shipboard and tactical operations.

6.0 Summary

Since its operational implementation at FNOC in January 1988, the MVOI analysis has become the workhorse in satisfying the Navy's many and diverse atmospheric analysis requirements. With only relatively minor modifications, the same software is used to perform the NOGAPS global analysis, the different NORAPS regional analyses, the global upper stratospheric analysis, the global low-level analysis, and limited-area and shipboard analyses wherever they are needed. Not only does this simplify software maintenance, but it also allows all of the Navy's operational analyses to simultaneously benefit from improvements realized through the latest research and development efforts.

The MVOI analysis has proven to be an especially effective and flexible vehicle for the assimilation of new types of observational and synthetically generated data into the Navy's atmospheric prediction systems. The incorporation of a new type of observation into the analysis is relatively straightforward, once the error properties and the spatial distribution of the data have been determined. This flexibility has been demonstrated by the operational implementation of the DMSP SSM/I wind speed data and several types of synthetic observations. For example, the synoptic skills of FNOC personnel are utilized to generate synthetic surface observations in the vicinity of oceanic extratropical cyclones that are poorly depicted by NOGAPS. Before admitting these observations into

the operational database, a limited-area NOGAPS analysis can be quickly run to ensure that the synthetic observations have the desired effect. The assimilation of these observations has significantly improved NOGAPS analyses and short-term forecasts for such cyclones. In the tropics, warning information issued by JTWC and NHC is used to create synthetic soundings in the vicinity of tropical storms. The assimilation of these observations into NOGAPS has been quite successful. Not only has it resulted in the improvement of the analyses and short-term forecasts for these storms, but it has also led to skillful 48-hour and 72-hour tropical storm forecasts from the global model (Fiorino et al., 1991).

Future efforts at NRL will concentrate on improved identification, tracking, and correction of erroneous observations and on refined estimates for the statistical parameters that affect the performance of the MVOI—in particular, the specification of the observation errors and the prediction errors. We expect to assimilate new data sources as they become available, and also plan to include a moisture analysis for NOGAPS. Finally, we are preparing the MVOI to run on the next-generation computer system, which will become operational at FNOC in the near future.

7.0 Acknowledgments

The successful development of the MVOI analysis is due primarily to the earlier work of E. Barker. The integration of the MVOI in the NOGAPS data assimilation system required the cooperation of the other NOGAPS team members—N. Baker, L. Brody, R. Gelaro, T. Hogan, and T. Rosmond. R. Hodur provided valuable assistance in the replacement of the NORAPS analysis with the MVOI. The original implementation of the MVOI at FNOC was made possible by the stalwart support of CDR R. Davies, USN (Ret.), and the late T. Hesse. The continued improvement of the MVOI and its many operational applications has been realized through the efforts of L. Clarke, C. Mauck, and G. Bayler, FNOC, and H. Lewit, Computer Sciences Corporation. We gratefully acknowledge the support of our sponsors, the Space and Naval Warfare Systems Command (PMW165), CAPT C. Hoffman, USN, Program Element 0603207N, and the Office of Naval Research, CDR L. Bounds, USN, Program Element 0602435N.

8.0 References

Baker, N. (1991). Quality Control of Meteorological Observations for the FNOC Operational Atmospheric Database. Naval Research Laboratory, Stennis Space Center, MS, NOARL Technical Note 144.

Barker, E. (1992). Design of the Navy's multivariate optimum interpolation analysis system. *Weather and Forecasting* 7, 220–231.

Barker, E. (1982). A Comparison of Two Initialization Methods in Data Assimilation. Naval Research Laboratory, Monterey, CA, NEPRF Technical Report TR 82-06.

Bergman, K. (1979). Multivariate analysis of temperature and winds using optimum interpolation. *Monthly Weather Review* 107, 1423–1444.

Bergthórssen, P. and B. Döös (1955). Numerical weather map analysis. *Tellus* 7, 329–340.

Buell, C. (1972). Correlation functions for wind and geopotential on isobaric surfaces. *J. Appl. Meteor.* 11, 51–59.

Carr, E. (1987). Objective data analysis conference. *Bull. Amer. Meteor. Soc.* 68, 481–484.

Clancy, R., P. Phoebus, and K. Pollak (1989). Technical Description of the Optimum Thermal Interpolation System, Version 1: A Model for Oceanographic Data Assimilation. Naval Research Laboratory, Stennis Space Center, MS, NORDA Report 240.

Cressman, G. (1959). An operational objective analysis system. *Monthly Weather Review* 87, 367–374.

Daley, R. (1985). The analysis of synoptic scale divergence by a statistical interpolation procedure. *Monthly Weather Review* 113, 1066–1079.

Daley R., A. Hollingsworth, J. Ploshay, K. Miyakoda, W. Baker, E. Kalnay, C. Dey, T. Krishnamurti, and E. Barker (1985). Objective analysis and assimilation techniques used for the production of FGGE IIIb analyses. *Bull. Amer. Meteor. Soc.* 77, 532–538.

Dey, C. (1989). The evolution of objective analysis methodology at the National Meteorological Center. *Weather and Forecasting* 4, 297–312.

DiMego, G. (1988). The National Meteorological Center regional analysis system. *Monthly Weather Review* 116, 977–1000.

Fiorino, M., J. Goerss, and J. Jensen (1991). An evaluation of tropical cyclone forecasting skill of the Navy Operational Global Atmospheric Prediction System. *Proc., 19th Conf. on Hurricanes and Tropical Meteorology,* Miami, Florida. Published by the American Meteorological Society, Boston, MA.

Franke, R. (1985). Sources of error in objective analysis. *Monthly Weather Review* 113, 260–270.

Franke, R., E. Barker, and J. Goerss (1988). The use of observed data for the initial-value problem in numerical weather prediction. *Comput. Math. Applic.* 16, 169–184.

Gandin, L. (1963). Objective analysis of meteorological fields. *Gidrommeteorologichoskoe Isdatel'stvo.,* Leningrad. [*Israel Program for Scientific Translations,* Jerusalem, 1965, 242 pp.]

Goerss, J. and P. Phoebus (1992). The Navy's Operational Atmospheric Analysis. *Weather and Forecasting* 7, 232–249.

Goerss, J. (1989). The impact of bogus observations upon the Navy Operational Global Atmospheric Prediction System. *Preprints, Twelfth Conference on Weather Analysis and Forecasting,* Monterey, CA. Published by the American Meteorological Society, Boston, MA, 41–45.

Goodberlet, M., C. Swift, and J. Wilkerson (1990). Ocean surface wind speed measurements of the Special Sensor Microwave/Imager (SSMI). *IEEE Transactions on Geoscience and Remote Sensing* 28, 823–828.

Guymer, L. (1978). Operational Application of Satellite Imagery to Synoptic Analysis in the Southern Hemisphere. Bureau of Meteorology, Melbourne, Australia, Tech. Rep. No. 26.

Haltiner, G. and F. Martin (1957). *Dynamical and Physical Meteorology*, McGraw-Hill Book Company, Inc.

Hodur, R. (1987). Evaluation of a regional model with an update cycle. *Monthly Weather Review* 115, 2707–2718.

Hogan, T., T. Rosmond, and R. Gelaro (1991). The Description of the Navy Operational Global Atmospheric Prediction System's Forecast Model. Naval Research Laboratory, Stennis Space Center, MS, NOARL Report 13.

Hollingsworth, A. and P. Lönnberg (1986). The statistical structure of short-range forecast errors as determined from radiosonde data. Part I: The wind field. *Tellus* 38A, 111–136.

Lönnberg, P. and A. Hollingsworth (1986). The statistical structure of short-range forecast errors as determined from radiosonde data. Part II: The covariance of height and wind errors. *Tellus* 38A, 137–161.

Lorenc, A. (1981). A global three-dimensional multivariate statistical interpolation scheme. *Monthly Weather Review* 109, 701–721.

McPherson, R., K. Bergman, R. Kistler, G. Rasch, and D. Gordon (1979). The NMC operational global data assimilation system. *Monthly Weather Review* 107, 1445–1461.

Mills, G. and R. Seaman (1990). The BMRC Regional Data Assimilation System. *Monthly Weather Review* 118, 1217–1237.

Nash, J. and F. Schmidlin (1987). WMO International Radiosonde Comparison, Final Report. WMO Instruments and Observing Methods Report No. 30, 103 pp.

Rosmond, T. (1981). NOGAPS: Navy Operational Global Atmospheric Prediction System. *Preprints, Fifth Conference on Numerical Weather Prediction*, Monterey, CA. Published by the American Meteorological Society, Boston, MA, 74–79.

Rosmond, T. (1992). The design and testing of the Navy Operational Global Atmospheric Prediction System. *Weather and Forecasting* 7, 262–272.

Rutherford I. (1976). An operational three-dimensional multivariate statistical objective analysis scheme. *Proceedings, Study Group Conference on Four-dimensional Data Assimilation*, Paris, 17–21 November 1975, GARP Report No. 11.

Shaw, D., P. Lönnberg, A. Hollingsworth, and P. Undén (1987). Data assimilation: The 1984/85 revisions of the ECMWF mass and wind analysis. *Quart. J. R. Met. Soc.* 113, 533–566.

Thiébaux, H., L. Morone, and R. Wobus (1990). Global forecast error correlation. Part 1: Isobaric wind and geopotential. *Monthly Weather Review* 118, 2117–2137.